Functional classification of *GNAI1* disorder variants in *C. elegans* uncovers conserved and cell-specific mechanisms of dysfunction

Rehab Salama[1], Eric Peet[1], Logan Morrione[1], Sarah Durant[1], Maxwell Seager[1], Madison Rennie[2], Suzanne Scarlata[2], and Inna Nechipurenko[1]

[1]Department of Biology and Biotechnology, Worcester Polytechnic Institute, Worcester, MA 01609

[2]Department of Chemistry and Biochemistry, Worcester Polytechnic Institute, Worcester, MA 01609

IN: inechipurenko@wpi.edu

Running title: *GNAI1* variants alter Gα protein function *in vivo*

Keywords: *GNAI1*, ODR-3, Gα proteins, cilia, neurodevelopmental disorders

ABSTRACT

Heterotrimeric G proteins transduce signals from G protein coupled receptors, which mediate key aspects of neuronal development and function. Mutations in the *GNAI1* gene, which encodes Gαi1, cause a disorder characterized by developmental delay, intellectual disability, hypotonia, and epilepsy. However, the mechanistic basis for this disorder remains unknown. Here, we show that *GNAI1* is required for ciliogenesis in human cells and use *C. elegans* as a whole-organism model to determine the functional impact of seven *GNAI1*-disorder patient variants. Using CRISPR-Cas9 editing in combination with robust cellular (cilia morphology) and behavioral (chemotaxis) assays, we find that *T48I*, *K272R*, *A328P*, and *V334E* orthologous variants impact both cilia assembly and function in AWC neurons, *M88V* and *I321T* have no impact on either phenotype, and *D175V* exerts neuron-specific effects on cilia-dependent sensory behaviors. Finally, we validate in human ciliated cell lines that *D173V*, *K270R*, and *A326P GNAI1* variants disrupt ciliary localization of the encoded human Gαi1 proteins similarly to their corresponding orthologous substitutions in the *C. elegans* ODR-3 (*D175V*, *K272R*, and *A328P*). Overall, our findings determine the *in vivo* effects of orthologous *GNAI1* variants and contribute to mechanistic understanding of *GNAI1* disorder pathogenesis as well as neuron-specific roles of ODR-3 in sensory biology.

44

45 **ARTICLE SUMMARY**

46 Gα subunits of heterotrimeric G proteins transduce signaling from G protein coupled
47 receptors and play important roles in cell communication and complex behaviors. Mutations in
48 the *GNAI1* gene, which encodes Gαi1 protein, have been recently linked to a
49 neurodevelopmental disorder; however, it remains unknown how *GNAI1* patient mutations
50 disrupt neuronal development or function to manifest in disease. We demonstrate that *GNAI1* is
51 required for ciliogenesis and use *C. elegans* as a whole-animal model in combination with
52 human cells to identify cell-specific and conserved mechanisms of Gα dysfunction.

53 **INTRODUCTION**

54 Heterotrimeric G proteins are key transducers of G protein coupled receptor (GPCR)
55 signaling, which plays key roles in neuronal development, communication, and behavior (Betke
56 et al., 2012; Kurabayashi et al., 2013; Wettschureck & Offermanns, 2005). In the canonical
57 GPCR cascade, the activated receptor acts as a guanine-nucleotide exchange factor (GEF) to
58 exchange guanosine diphosphate (GDP) on the Gα subunit of the Gαβγ trimer for guanosine
59 triphosphate (GTP), thus stimulating dissociation of Gα-GTP from Gβγ and allowing activation of
60 their respective downstream effectors (Dror et al., 2015; Gilman, 1987; Pierce et al., 2002).

61 Many GPCRs, G proteins, and their downstream effectors localize to primary cilia –
62 specialized cellular compartments that house molecular machinery of all major signaling
63 pathways (Anvarian et al., 2019; Hilgendorf et al., 2016). Primary cilia mediate many aspects of
64 neuronal biology in the developing and mature brain including cell fate specification,
65 proliferation, migration, axon guidance, dendrite morphogenesis, and neuronal excitability
66 (Hasenpusch-Theil & Theil, 2021; Jurisch-Yaksi et al., 2024; Stoufflet & Caille, 2022; Suciu &
67 Caspary, 2021). In humans, cilia dysfunction is associated with a spectrum of developmental

68 disorders called ciliopathies (Hildebrandt et al., 2011; Reiter & Leroux, 2017). Ciliopathy patients
69 commonly exhibit neurological symptoms that range in severity and include structural brain
70 abnormalities, intellectual disability, motor deficits, and epilepsy (Guemez-Gamboa et al., 2014;
71 Lee & Gleeson, 2011; Valente et al., 2014), further highlighting the critical importance of primary
72 cilia in the nervous system. In addition to classic ciliopathies, cilia defects are being increasingly
73 reported in neurodevelopmental, neurodegenerative, and psychiatric disorders suggesting that
74 cilia dysfunction may be a shared feature of many neurological conditions (Jurisch-Yaksi et al.,
75 2024; Karalis et al., 2022). However, the mechanisms by which cilia dysfunction contributes to
76 neurological phenotypes observed in these disorders or those by which risk genes for these
77 disorders impact cilia biology remain largely unknown.

78 Recent studies identified >15 *de novo* mutations in the *GNAI1* gene, which encodes the
79 Gαi1 subunit of heterotrimeric G (αβγ) proteins, in individuals with a novel neurodevelopmental
80 disorder (NDD) henceforth referred to as '*GNAI1* disorder' (Muir et al., 2021). Most affected
81 individuals exhibited developmental delay, intellectual disability, hypotonia, and epilepsy –
82 neurological symptoms that are also commonly associated with classic ciliopathies. Although
83 the mechanistic basis for *GNAI1* disorder remains unknown, prior studies have described
84 several neuronal functions for Gαi1. In the canonical GPCR cascade, Gαi1 is responsible for
85 decreasing cAMP levels upon receptor activation by inhibiting adenylyl cyclases (Wettschureck
86 & Offermanns, 2005). Acute *GNAI1* knockdown in the mouse embryonic cortex disrupted
87 multiple aspects of cortical development including progenitor proliferation, neuronal migration,
88 and dendritogenesis (Hamada et al., 2021). Additionally, genetic ablation of *GNAI1* has been
89 reported to increase adenylyl cyclase activity and impair hippocampus-dependent long-term
90 memory in mice (Pineda et al., 2004). While the cellular and molecular mechanisms that
91 underlie neuronal functions of Gαi1 remain to be fully elucidated, these studies demonstrate that
92 Gαi1 plays critical roles both in the developing and mature brain and underscore the importance

93 of understanding the functional effects of *GNAI1* patient variants in relevant cellular and
94 developmental contexts *in vivo*.

95 *C. elegans* constitutes a powerful whole-organism platform for rapidly evaluating
96 phenotypic consequences of NDD-associated missense variants. Several recent studies
97 successfully deployed *C. elegans* to functionally classify *de novo* variants in risk genes for
98 developmental disorders that include *GNAO1* encephalopathy (Wang et al., 2022), autism
99 spectrum disorder (Wong et al., 2019), and ciliopathies (Lange et al., 2022; Lange et al., 2021).
100 Here, we use *C. elegans* ODR-3, which belongs to the Gαi/o class of G proteins, as a model to
101 evaluate the functional impacts of seven NDD-associated *GNAI1* variants. Using *C. elegans*
102 ODR-3 for this purpose offers several key advantages. First, all missense variants selected for
103 analysis alter amino acids that are identical between Gαi1 and ODR-3 and map to the functional
104 motifs conserved across Gα proteins. Second, *odr-3* loss-of-function (lf) and gain-of-function (gf)
105 mutations result in robust and easily quantifiable cellular phenotypes – defects in cilia
106 morphology in AWA and AWC olfactory neurons (Campagna et al., 2023; Lans et al., 2004;
107 Roayaie et al., 1998). Finally, *odr-3* function is required for a panel of chemosensory behaviors
108 including avoidance of high-osmolarity solutions detected by ASH and chemotaxis toward
109 attractive odorants detected by AWA and AWC neurons (Bargmann et al., 1993; Roayaie et al.,
110 1998). As a result, a complementary approach combining robust cellular and behavioral assays
111 can be used to rapidly identify gene variants that are functionally consequential *in vivo*.

112 We find that five of the examined orthologous variants exhibited a range of defects in
113 AWC cilia morphology and/or AWC-mediated attraction to benzaldehyde, while two variants
114 appeared wild-type in both assays. Interestingly, one examined variant had cell-specific effects
115 on neuronal function - a marked deficit in ASH-mediated glycerol avoidance and unaltered
116 AWC-mediated chemotaxis toward benzaldehyde. Finally, we confirm that the functional impact

117 of three orthologous variants that severely compromised localization of the encoded ODR-3
118 proteins to AWC cilia is conserved in human cells.

119 MATERIALS AND METHODS

120 *C. elegans* strains and maintenance

121 All *C. elegans* strains were maintained at 15°C or 20°C on nematode growth medium
122 (NGM) agar plates seeded with *Escherichia coli* OP50 (Brenner, 1974). Standard genetic
123 techniques were used to generate all strains. PCR and/or Sanger sequencing was used to
124 confirm genotypes of all mutant strains. Transgenic *C. elegans* carrying multicopy
125 extrachromosomal arrays were generated by germline transformation. To generate transgenic
126 strains, experimental plasmids were microinjected at 5 – 10 ng/μl together with either *unc-*
127 *122*Δp*::gfp* or *unc-122*Δp*::dsred* co-injection markers injected at 30 ng/μL and 40 ng/μL,
128 respectively. Wild-type and all mutant TagRFP-tagged *odr-3* constructs were injected at
129 identical concentrations. Two or more independently generated lines were examined for all
130 extrachromosomal transgenes, and the same extrachromosomal array was examined in wild-
131 type and mutant backgrounds that were being directly compared. A list of *C. elegans* strains
132 used in this study is provided in Supplementary Table 1.

133 Chemotaxis behavioral assays

134 Population chemotaxis assays were performed on 10-cm round petri plates as
135 previously described (Bargmann et al., 1993; Campagna et al., 2023). Briefly, 1 μL of
136 benzaldehyde (Sigma) diluted in ethanol at 1:200 and 1 μL of ethanol (diluent control) were
137 placed along with 1 μL of 1M sodium azide anesthetic at opposite ends of the assay plate.
138 Young adult hermaphrodites were washed off their growth plates with cholesterol-free S-basal,
139 washed twice with S-basal, once with Milli-Q water, and transferred to assay plates. After one
140 hour, chemotaxis index was calculated as follows:

141 CI = (# worms at attractant – # worms at ethanol)/total worms that left origin

142 All assays were performed on three or more days with at least two technical replicates per
143 genotype per day. Wild-type and *odr-3(lf)* controls were included with experimental genotypes
144 on all days of the assay.

145 **Osmotic avoidance assays**

146 Osmotic avoidance assays were performed as previously described (Cornils et al., 2016;
147 Culotti & Russell, 1978). Briefly, 4-6 one-day old hermaphrodites were transferred from a growth
148 plate onto an NGM plate without food for 2 minutes to remove residual *E. coli* OP50. The same
149 animals were subsequently placed inside a ring (~3/8th inch in diameter) of 8M glycerol colored
150 with bromophenol blue (USB). After 2 minutes, the number of animals that remained inside the
151 glycerol ring was counted. All assays were repeated on five or more separate days with at least
152 three technical replicates per genotype per day. Wild-type and *odr-3(lf)* controls were included
153 with experimental genotypes on all days of the assay.

154 **CRISPR-Cas9 gene editing**

155 Cas9 protein, crRNAs, and tracrRNA were purchased from Integrated DNA
156 Technologies (IDT). All missense mutations and insertion of the split-wrmScarlet (wrmScarlet$_{11}$)
157 tag were confirmed by Sanger sequencing.

158 *Generation of missense odr-3 variants*: gene editing was carried out as described in
159 (Dokshin et al., 2018). Briefly, donor oligonucleotides carrying the desired missense mutations,
160 silent mutations within the crRNA target sequence and/or PAM site to prevent repetitive cutting,
161 and 36-40 bp homology arms were ordered from IDT (see Supplementary Fig. 4 for detailed
162 sequence information). The donor template (25 ng/μL), crRNA (56 ng/μL), tracrRNA (100
163 ng/μL), and Cas9 protein (250 ng/μL) were co-injected with *unc-122Δ*p*::dsred* or *unc-122Δ*p*::gfp*
164 co-injection markers, and F1 progeny expressing the co-injection marker were isolated and

165 genotyped for the presence of the edit. F2 individuals homozygous for the desired mutation
166 were subsequently isolated from heterozygous F1 parents. All mutants generated via CRISRP-
167 Cas9 editing were sequenced by Sanger sequencing and outcrossed at least two times to
168 mitigate potential off-target effects.

169 *Generation of wrmScarlet$_{11}$ knock-in strain*: To generate the split-wrmScarlet
170 (*wrmScarlet$_{11}$*) allele *odr-3(nch013),* a single-stranded donor oligonucleotide containing the
171 *wrmScarlet$_{11}$* fragment (Goudeau et al., 2021), linkers, and homology arms was synthesized by
172 IDT. *wrmScarlet$_{11}$* sequence was inserted between codons encoding Gly118 and Glu119
173 residues of ODR-3 (Campagna et al., 2023).

174 crRNA: 5' GTACAGGAAAATGGAGAAGA 3'

175 donor oligonucleotide: 5'
176 AAGAAGCAGAAAAGGCAATAGTTATGAAAGTACAGGAAAAcGGcGAgGAAGGAAGTGGAGG
177 AGGAGGAAGTTACACCGTCGTCGAGCAATACGAGAAGTCCGTCGCCCGTCACTGCACCGG
178 AGGAATGGATGAGTTATACAAGAGTGGAGGAGGAGGAAGTGAAGCACTGACAGAAGAAGT
179 TTCGAAAGCAATTCAATCG 3'

180 **Molecular biology**

181 *odr-3 mutant constructs*: expression of *odr-3* transgenes in AWC and ASH was achieved
182 by sub-cloning *odr-3* cDNA downstream from 0.7 kb of *ceh-36* (*ceh-36*Δp) (Kim et al., 2010) and
183 ~3 kb of *sra-6* (*sra-6*p) regulatory sequences, respectively. TagRFP tag was inserted between
184 Gly118 and Glu119 residues of ODR-3 as previously described (Campagna et al., 2023).
185 Patient mutations were introduced into plasmids carrying wild-type *tagrfp*-tagged *odr-3* cDNA
186 downstream from cell-specific promoters by site-directed mutagenesis using QuikChange
187 Lightning kit (Agilent Technologies). All constructs were verified by whole-plasmid sequencing
188 (Plasmidsaurus).

189 *GNAI1 constructs*: wild-type coding sequence of human *GNAI1* (NM 002069) cloned into
190 *pcDNA3.1+* (Invitrogen) mammalian expression vector was purchased from Bloomsburg
191 University Foundation cDNA Resource Center (Catalog # GNAI100000). *eGFP* coding
192 sequence with flanking DNA segments encoding GlyThr (5' linker) and GlySer (3' linker) was
193 inserted between Leu91 and Lys92 of *GNAI1* coding sequence in *pcDNA3.1+* vector using
194 NEBuilder HiFi DNA assembly (NEB) to make *eGFP*-tagged *GNAI1* construct. Missense
195 mutations corresponding to *D173V*, *K270R*, and *A326P* substitutions were introduced into the
196 *pcDNA3.1+* plasmid containing *eGFP*-tagged *GNAI1* via site-directed mutagenesis using
197 QuikChange Lightning kit (Agilent Technologies). All constructs were verified by full-plasmid
198 sequencing (Plasmidsaurus). A list of plasmids used in this work is provided in Supplementary
199 Table 2.

200 *qPCR*: total RNA was extracted from siControl and si*GNAI1*-treated RPE-1 and
201 HEK293T cells using RNeasy kit (Qiagen) per manufacturer's instructions. RNA samples were
202 reverse-transcribed (ZymoScript One-Step RT-qPCR Kit), and *GNAI1* expression (relative to
203 *RPL11* control) was quantified by real-time PCR carried out on Applied Biosystems QuantStudio
204 6 Pro system using the $2^{-\Delta\Delta Ct}$ method. Primer pairs used in this study are below:

205 *RPL11*: 5' GTTGGGGAGAGTGGAGACAG 3' / 5' TGCCAAAGGATCTGACAGTG 3'

206 *GNAI1*: 5' CCCGAGAGTACCAGCTTAATG 3' / 5' CATCTTGTTGAGTCGGGATGTA 3'

207 **Cell culture and transfections**

208 All cell lines were maintained at 37°C with 5% CO_2 and tested monthly for mycoplasma
209 using mycoplasma PCR detection kit (ABM). Human telomerase-immortalized retinal pigment
210 epithelial cells (hTERT RPE-1 (Nechipurenko et al., 2016)) were cultured in DMEM/F-12 (1:1)
211 supplemented with 10% fetal bovine serum (FBS) and 1X antibiotic-antimycotic (Gibco).

212 HEK293T cells (Abcam) were grown in DMEM high-glucose supplemented with Glutamax
213 (Gibco), 10% FBS, and 1X antibiotic-antimycotic (Gibco).

214 *RNAi:* For immunofluorescence analysis, RPE-1 and HEK293T cells were plated on 12-
215 mm glass pre-treated or Poly-D-Lysine-coated coverslips (Neuvitro), respectively, in 24-well
216 plates at 30,000 cells per well in antibiotic-free complete-growth medium. For qPCR analysis,
217 cells were plated without coverslips in 12-well plates at 60,000 cells per well. Synthetic small
218 interfering RNA oligonucleotides (siRNAs) targeting non-overlapping *GNAI1* sequences or non-
219 targeting control siRNA were transfected as previously described (Nechipurenko et al., 2016)
220 using Lipofectamine RNAiMax (Invitrogen). The target sequences and sources of siRNAs used
221 in this study are provided below:

222 si*GNAI1* #1 (s5872, Ambion): GAAUUGUUGAAACCCAUUU

223 si*GNAI1* #2 (J-010404-07-0002, Dharmacon): CAAAUUACAUCCCGACUCA

224 siControl (D-001810-01-05, Dharmacon): UGGUUUACAUGUCGACUAA

225 *Transfection of GNAI1 plasmids:* HEK293T cells were plated on 12-mm glass Poly-D-
226 Lysine-coated coverslips (Neuvitro) in 24-well plates at 30,000 cells per well in antibiotic-free
227 complete-growth medium. Upon reaching 50-60% confluence, the plated cells were transfected
228 with 500 ng of pcDNA3.1+ vector containing eGFP-tagged $GNAI1^{WT}$, $GNAI1^{D173V}$, $GNAI1^{K270R}$, or
229 $GNAI1^{A326P}$ using Lipofectamine 3000 (Invitrogen) per manufacturer's instructions. After a three-
230 day incubation period, the transfection medium was replaced with serum-free medium to induce
231 ciliation. Cells were serum-starved for 48 hrs prior to fixation and analysis.

232 **Immunostaining**

233 RPE-1 and HEK293T cells were fixed in 4% paraformaldehyde for 12 minutes followed
234 by permeabilization in 0.2% Triton X-100 (MP Biomedicals) for 10 minutes at room temperature

235 (RT). Fixed cells were blocked with 5% bovine serum albumin in phosphate buffered saline
236 (PBS) with 0.2% Triton X-100 (PBS-T) for 1 hour at RT or at 4°C overnight, followed by
237 incubation in primary antibodies for 1.5 hours at RT or at 4°C overnight. The following
238 antibodies were used in immunofluorescence experiments: anti-γ-tubulin (clone 8D11, 1:500,
239 Biorbyt, batch # T1578), anti-ARL13B (clone N295B/66, 1:10, Developmental Studies
240 Hybridoma Bank), anti-acetylated α-tubulin (clone 6-11B-1, 1:500, Sigma, batch # T7451), anti-
241 GFP (catalog # GFP-1010, 1:500, Aves Laboratories, batch # GFP917979), and anti-
242 GM130/GOLGA2 (catalog # HPA021178, 1:500, Sigma, batch # A105115). Species-specific
243 fluorescent secondary antibodies were obtained from Jackson ImmunoResearch laboratories
244 and used at 1:500 dilution in PBS-T. DAPI (1:1000, ThermoFisher) was used to stain DNA and
245 applied together with secondary antibodies for 1.5 hours at RT or at 4°C overnight.

246 **Microscopy**

247 *C. elegans*: Synchronized one-day old adult hermaphrodites were anesthetized in 10mM
248 tetramisole hydrochloride (MP Biomedicals) and placed on a 10% agarose pad mounted on a
249 microscope slide. Animals were imaged on an upright THUNDER Imager 3D Tissue (Leica).
250 Complete z-stacks of AWC and ASH sensory endings that included distal dendrite and cilia
251 were acquired at 0.22-µm intervals with a K5 sCMOS camera (Leica) in Leica Application Suite
252 X software using an HC Plan Apochromat 63X NA 1.4–0.60 oil immersion objective. To image
253 one-day-old split-wrmScarlet transgenic animals, single-plane snapshots were acquired on an
254 inverted Nikon Ti-E microscope with Yokogawa CSU-X1 spinning disk confocal head using 60X
255 NA 1.40 oil immersion objective.

256 *RPE-1 and HEK293T cells*: Fixed and stained RPE-1 and HEK293T cells were mounted
257 in ProLong Diamond antifade mountant (Invitrogen) and imaged on an inverted Nikon Ti-E
258 microscope with Yokogawa CSU-X1 spinning disk confocal head using a 60X NA 1.40 oil

259 immersion objective. Complete z-stacks were acquired at 0.25-µm intervals with an ORCA-
260 Fusion BT Digital CMOS camera (Hamamatsu) in MetaMorph 7 software (Molecular devices).

261 **Image analysis**

262 Analysis of all fluorescence microscopy images was performed in Fiji/Image J (National
263 Institute of Health, Bethesda, MD). All data were quantified from images collected on at least
264 two independent days. For experiments examining localization of TagRFP-tagged ODR-3
265 variants and eGFP-tagged Gαi1 variants, all genotypes/conditions being compared directly were
266 imaged at identical settings.

267 *ODR-3::TagRFP fluorescence intensity (AWC and ASH):* TagRFP fluorescence intensity
268 inside AWC cilia or PCMC in the distal dendrite was measured by outlining AWC cilia or PCMC
269 using the freehand selection tool and measuring mean intensity inside the resultant ROIs. The
270 relative fluorescence intensity was plotted as a ratio of mean TagRFP intensity inside the AWC
271 cilium over mean TagRFP intensity inside the PCMC of the same neuron. TagRFP fluorescence
272 intensity inside ASH cilium was measured by drawing a line segment along the center of the
273 ASH cilium (from base to tip) and measuring mean intensity along the line. TagRFP intensity
274 inside the PCMC of ASH was measured as described above for AWC, and the relative intensity
275 was calculated and plotted as a ratio of intensity inside the ASH cilium over intensity in the
276 PCMC of the same neuron.

277 *Cilia area (AWC)*: The area of AWC cilia was measured as previously described
278 (Campagna et al., 2023). Briefly, the cilia were outlined using the freehand selection tool, and
279 the area enclosed by the ROI was measured from maximum-intensity projections that contained
280 AWC cilia in their entirety.

281 *Gαi1::eGFP relative fluorescence intensity*: Line segments were drawn from base to tip,
282 along the center of the cilia, visualized using anti-ARL13B antibody, and mean intensity along

283 the line was measured in the eGFP channel in transfected HEK293T cells. Another straight line
284 was drawn across the Golgi visualized with anti-GOLGA2 antibody, and mean intensity along
285 the line was measured in the eGFP channel. The relative Gαi1::eGFP intensity was calculated
286 and plotted as a ratio of eGFP intensity inside the cilium over eGFP intensity in the Golgi of the
287 same transfected cell.

288 **Statistical analysis**

289 Prism 10 software (GraphPad, San Diego, CA) was used to perform all statistical
290 analyses and generate bar graphs and scatter plots. The D'Agostino-Pearson test was used to
291 determine whether the data were normally distributed. Details on the numbers of analyzed
292 animals and cells, statistical tests, and multiple comparison correction (when applicable) are
293 presented in figure legends.

294 **RESULTS**

295 ***GNAI1* is required for ciliogenesis in mammalian cells**

296 Given the overlap in clinical features observed in classic ciliopathies and *GNAI1* disorder
297 (Neurodevelopmental disorder with hypotonia, impaired speech, and behavioral abnormalities;
298 OMIM # 619854), we first wondered whether *GNAI1* may play a role in cilia assembly. To
299 address this question, we knocked down *GNAI1* in human embryonic kidney (HEK293T) and
300 immortalized retinal pigment epithelial (hTERT RPE-1) cells – two commonly used cell culture
301 models in cilia research. Roughly 80% of RPE-1 cells transfected with non-targeting control
302 siRNA (*si*Control) possessed a primary cilium labeled with anti-ARL13B antibody; however, only
303 34% of cells transfected with si*GNAI1* (si*GNAI1 #1*) that targets both *GNAI1* reference
304 transcripts (NM 001256414.1 and NM 002069.5) were ciliated (Fig. 1a and c), suggesting that
305 *GNAI1* is required for ciliogenesis in RPE-1 cells. Importantly, RPE-1 cells transfected with the
306 second siRNA that targets a distinct non-overlapping region of *GNAI1* (si*GNAI1* #2) resulted in a

307 similar knockdown efficiency and ciliation defect (Supplementary Fig. 1 a and b), suggesting
308 that the observed cilia phenotype is likely *GNAI1*-dependent. To confirm that reduction in cilia
309 number observed upon *GNAI1* KD is not simply due to defective ciliary trafficking of ARL13B,
310 we stained *GNAI1* KD RPE-1 cells with an antibody against acetylated tubulin, which labels the
311 axoneme, and noted a comparable reduction in number of ciliated cells (Supplementary Fig. 1 c
312 and d).

313 To test if *GNAI1* function is broadly required for ciliogensis in human cells, we next
314 turned to HEK293T cells. Similarly to RPE-1 cells, *GNAI1* KD in HEK293T cells caused a
315 significant reduction in ciliogenesis (Fig. 1b and d). However, the overall impact of *GNAI1* KD on
316 ciliation of HEK293T cells appeared to be qualitatively milder relative to RPE-1 cells (compare
317 Fig. 1c and Fig. 1d), despite similar *GNAI1* KD efficiency in both cell lines (Fig. 1e), indicating
318 that *GNAI1* may differentially contribute to cilia assembly in different cell types.

319 **Selection of *GNAI1* disorder variants for *in vivo* functional analysis**

320 Sequence analysis determined that *C. elegans* ODR-3 exhibits 49% amino acid
321 sequence identity and 66% similarity to human Gαi1 (100% length, EMBOSS Needle; BLAST e-
322 value $6x10^{-127}$; Supplementary Fig. 2). The majority of *GNAI1* disorder missense variants impact
323 residues in the protein domains conserved across all Gα proteins (Muir et al., 2021). Therefore,
324 we reasoned that we could leverage the well defined genetics of *odr-3* together with robust
325 cellular and behavioral phenotypes displayed by *odr-3(lf)* and *odr-3(gf)* mutants to determine
326 functional impacts of select *GNAI1* patient variants *in vivo*. To this end, we chose to focus on
327 seven missense *GNAI1* alleles that affect conserved, identical amino acids in ODR-3 (Fig. 2a
328 and b; Supplementary Fig. 2). Four mutations (*GNAI1*: *T48I*, *D173V*, *K270R*, and *A326P*) map
329 to structurally conserved motifs called G boxes that mediate binding and hydrolysis of guanine
330 nucleotides (Luo et al., 2022; Noel et al., 1993; Sprang, 1997), one mutation (*GNAI1*: *V332E*)
331 impacts a residue in the C-terminal alpha-helix, which participates in Gα interactions with

332 GPCRs (Masuho et al., 2023; Oldham et al., 2006) and cytoplasmic GEF RIC-8 (Kant et al.,
333 2016; Seven et al., 2020; Zeng et al., 2019), and two mutations (*GNAI1*: *M88V* and *I319T*) are
334 in the conserved residues outside of known functional domains (Fig. 2a and b).

335 **_GNAI1_ disorder-associated orthologous variants differentially impact ODR-3 ciliary**
336 **localization**

337 Previous studies used overexpressed ODR-3 transgenes and immunofluorescence
338 against endogenous ODR-3 to demonstrate that wild-type ODR-3 (ODR-3^{WT}) is normally
339 enriched in the cilia of AWC sensory neurons (Roayaie et al., 1998). First, we wanted to
340 determine whether any of the selected variants affect sub-cellular localization of ODR-3. To
341 address this question, we first tagged the *odr-3* locus with split-wrmScarlet reporter
342 (*wrmScarlet*$_{11}$) (Goudeau et al., 2021) using CRISPR-Cas9 genome editing. To visualize
343 endogenous ODR-3 in AWC cilia, we reconstituted fluorescence via expression of the
344 wrmScarlet$_{1-10}$ fragment in AWC neurons under the *ceh-36Δ* promoter (Kim et al., 2010).
345 Consistent with published studies, ODR-3^{WT}::split-wrmScarlet was enriched inside AWC cilia
346 (n=25 animals, Supplementary Fig. 3). However, the reconstituted wrmScarlet was
347 photobleached nearly instantaneously upon sample illumination with the laser light making it
348 impossible to acquire multiple *z*-slices necessary for in-depth quantitative analysis of ODR-3
349 subcellular localization.

350 To bypass the photobleaching issue, we next expressed TagRFP-tagged wild-type or
351 mutant ODR-3 variants from transgenes in AWC neurons of wild-type animals and examined
352 cilia localization of the encoded proteins. Similarly to the endogenous ODR-3, ODR-
353 3^{WT}::TagRFP expressed from a multicopy transgene was enriched in AWC cilia (Campagna et
354 al., 2023) (Fig. 3a). We noted no significant changes in sub-cellular localization of TagRFP-
355 tagged ODR-3^{I321T} or ODR-3^{V334E} variants (Fig. 3a and b). Interestingly, we observed two distinct
356 patterns of mislocalization amongst the remaining ODR-3 protein variants. Like ODR-3^{WT}, ODR-

357 3^{T48I} and ODR-3^{M88V} were present inside the AWC cilium. However, unlike the WT protein, these
358 variants were also detected in an ectopic pool in the periciliary membrane compartment (PCMC)
359 of the distal dendrite (Fig. 3a and b). Finally, ODR-3^{D175V}, ODR-3^{K272R}, and ODR-3^{A328P} exhibited
360 the most striking defects in sub-cellular localization – these mutant proteins were largely
361 excluded from the AWC cilium and instead accumulated in the PCMC (Fig. 3a and b).

362 To rule out the possibility that dendritic mislocalization observed with the mutant variants
363 was an artifact of transgene overexpression, we introduced *A328P* mutation into the *odr-3::split-*
364 *wrmScarlet* background. The endogenously tagged ODR-3^{A328P}::split-wrmScarlet exhibited cilia
365 localization defects that were qualitatively similar to those observed in transgenic animals
366 overexpressing ODR-3^{A328P}::TagRFP in AWC neurons (Supplementary Fig. 3). Specifically,
367 ODR-3^{A328P}::split-wrmScarlet was present throughout the AWC dendrite in all examined animals
368 (n=30) and prominently accumulated at the cilia base in 28 out of 30 analyzed animals
369 (Supplementary Fig. 3). Collectively, these data indicate that *T48I*, *M88V*, *D175V*, *K272R*, and
370 *A328P* variants affect ciliary trafficking of the encoded ODR-3 proteins, with the latter three
371 mutations having the most profound impact on ODR-3 ciliary localization.

372 **The transition zone contributes to ciliary exclusion of the ODR-3^{A328P} protein**

373 Protein trafficking in and out of primary cilia is tightly controlled by the transition zone
374 (TZ) – a selective diffusion barrier at the cilia base (Garcia-Gonzalo & Reiter, 2017). One
375 possible explanation for the exclusion of ODR-3^{A328P} from the AWC cilium with a concomitant
376 accumulation in the distal dendrite is that *A328P* mutation impedes ODR-3 transport into the
377 cilium across the TZ. If this hypothesis were true, we would expect to see an increase in intra-
378 ciliary levels of ODR-3^{A328P} protein in animals with disrupted TZ architecture compared to wild
379 type. To test this hypothesis, we examined ODR-3^{A328P} localization in *mks-5(tm3100)* mutants
380 that have compromised TZ integrity (Jensen et al., 2015). In line with our hypothesis, we noted
381 an increase in ODR-3^{A328P}::TagRFP levels inside the cilium relative to distal dendrite in *mks-*

382 *5(tm3100)* mutants compared to ODR-3^{A328P}::TagRFP levels in the wild-type background (Fig.
383 4a and b). Notably, when we examined localization of ODR-3^{WT}::TagRFP in *mks-5(tm3100)*
384 mutants, we noticed that in addition to cilia, ODR-3^{WT}::TagRFP was now present in the distal
385 dendrite, consistent with the previously published role for the TZ in preventing leakage of
386 membrane-associated ciliary proteins into the dendrite (Cevik et al., 2013). Collectively, our
387 results suggest that the TZ plays an important part in regulating ODR-3 ciliary entry and
388 retention, and that the *A328P* variant likely impacts ODR-3 trafficking across the TZ.

389 **_odr-3_ mutations orthologous to patient _GNAI1_ variants differentially affect AWC cilia**
390 **morphology**

391 To gain insight into the functional effects of the *GNAI1* disorder-associated variants *in*
392 *vivo*, we used CRISPR-Cas9 editing to engineer worms homozygous for orthologous variants in
393 the *odr-3* gene (Supplementary Fig. 4 and Supplementary Fig. 5). To visualize AWC cilia
394 morphology, which is dependent on intact *odr-3* function, we then crossed an AWC-specific *gfp*
395 reporter into the CRISPR-Cas9-engineered *odr-3* mutant strains. Consistent with published
396 work, *odr-3(lf)* animals exhibited marked reduction in AWC cilia size compared to wild type (Fig.
397 5a and b). Cilia appeared normal in *M88V* and *I321T* homozygous animals (Fig. 5a and b). On
398 the other hand, *T48I*, *D175V*, *A328P*, and *V334E* mutants exhibited cilia defects that ranged
399 from mild albeit significant reduction in cilia size in *T48I* and *V334E* mutants to markedly smaller
400 cilia in *D175V* and *A328P* mutants (Fig. 5a and b). Notably, the cilia phenotype in *A328P*
401 animals was qualitatively and quantitatively indistinguishable from that of *odr-3(lf)* mutants,
402 suggesting that *A328P* allele may be a functional null. Re-expression of wild-type *odr-3* in AWC
403 neurons of *A328P* mutant animals partially but significantly rescued AWC cilia morphology (Fig.
404 5a and b), indicating that cilia defects in *A328P* mutants are indeed due to the loss of *odr-3*
405 function. Despite multiple attempts, we were unable to engineer a *K272R* variant in the *odr-3*
406 gene; so we took an alternative approach to determine whether this mutation impacts *odr-3*

407 function. Specifically, we overexpressed ODR-3^{K272R} cDNA in AWC neurons of *odr-3(lf)* animals
408 and quantified AWC cilia size in the transgenic animals. We found that these transgenic worms
409 were indistinguishable from *odr-3(lf)* mutants (Fig. 5a and b), suggesting that *K272R* mutation
410 strongly impairs ODR-3 activity.

411 *K272R* and *A328P* – two mutations that result in most severe cilia defects – alter
412 conserved amino acids that come into direct contact with GDP/GTP. Lysine 272 participates in
413 guanosine recognition (Luo et al., 2022), while alanine 328 is found in the TCAT motif, which is
414 conserved throughout the G protein family, and forms a hydrogen bond with the oxygen in
415 guanine (Luo et al., 2022). Therefore, cilia morphology defects observed in *K272R* and *A328P*
416 mutants likely stem from aberrant interaction of ODR-3 with guanosine nucleotides.

417 **The *A328P* variant does not abolish ODR-3 interaction with RIC-8 or UNC-119**

418 We previously showed that ODR-3 function is regulated by the cytoplasmic GEF and
419 chaperone RIC-8 (Campagna et al., 2023). Like *odr-3(lf)* and *A328P* mutants, *ric-8(lf)* mutants
420 exhibit a marked reduction in AWC cilia size. Since the *A328P* variant alters a residue just
421 proximal to the Gα α5 helix, which participates in Gα – RIC-8 binding (Kant et al., 2016; Zeng et
422 al., 2019), we next wanted to test whether this variant may impact cilia morphology by
423 interfering with the ODR-3 – RIC-8 interaction. To address this question, we first examined *in*
424 *vivo* association between ODR-3^{A328P} and RIC-8 via bimolecular fluorescence complementation
425 (BiFC) (Shyu et al., 2008) and found that both ODR-3^{WT} and ODR-3^{A328P} variants tagged with
426 the N-terminal Venus fragment (VN) associated with RIC-8 that was tagged with the C-terminal
427 half of Venus (VC) (Supplementary Fig. 6a and b). Since BiFC is irreversible and may increase
428 the likelihood of false positives over time (Kerppola, 2008; Xing et al., 2016), we next turned to
429 FRET-FLIM (Algar et al., 2019) to confirm that ODR-3^{A328P} does indeed bind RIC-8 *in vivo*. We
430 expressed GFP-fused RIC-8 alone or together with TagRFP-tagged ODR-3^{WT} or ODR-3^{A328P}
431 constructs in AWC neurons under the ceh-36Δ promoter. As compared to RIC-8::GFP alone,

432 the lifetime of GFP decreased in animals co-expressing RIC-8::GFP with ODR-3^{WT} confirming
433 interaction between the two proteins (Supplementary Fig. 6c and d). Comparable reduction in
434 GFP lifetime was also observed when we co-expressed RIC-8::GFP with ODR-3^{A328P}
435 (Supplementary Fig. 6c and d), suggesting that *A328P* substitution does not abolish the
436 association of the mutant ODR-3 with RIC-8, consistent with our BiFC data.

437 The GTP/GDP exchange cycle was also proposed to regulate the interaction between
438 Gα proteins and an evolutionarily conserved trafficking adaptor UNC-119, which plays a key
439 role in transporting Gα proteins to cilia (Zhang et al., 2011). Studies in mice and *C. elegans*
440 demonstrated that *unc-119* deletion causes Gα protein mislocalization in sensory neurons of
441 both species (Zhang et al., 2011). Furthermore, knocking down or mutating *unc-119* in zebrafish
442 and *C. elegans*, respectively, produced phenotypes consistent with aberrant cilia function
443 (Wright et al., 2011). So next we wondered whether *A328P* variant may disrupt ODR-3
444 interaction with UNC-119, as loss of this association could explain accumulation of ODR-3^{A328P}
445 protein in the dendrite as well as cilia defects observed in *A328P* mutants. We expressed UNC-
446 119 tagged with the C-terminal fragment of Venus (VC::UNC-119) together with either ODR-3^{WT}
447 or ODR-3^{A328P} tagged with the N-terminal Venus fragment (ODR-3^{WT}::VN and ODR-3^{A328P}::VN,
448 respectively) in AWC neurons of wild-type animals. We observed BiFC in 28% of animals co-
449 expressing VC::UNC-119 and free N-terminal Venus fragment (negative control)
450 (Supplementary Fig. 7). Co-expression of VC::UNC-119 with ODR-3^{WT}::VN or ODR-3^{A328P}::VN
451 reconstituted fluorescent signal in AWC neurons of a significantly greater percent of transgenic
452 animals (81% and 51%, respectively) (Supplementary Fig. 7b), indicating that ODR-3^{A328P}
453 retains ability to interact with UNC-119. However, the BiFC signal in animals co-expressing
454 VC::UNC-119 with ODR-3^{A328P}::VN appeared to concentrate at the cilia base and was
455 qualitatively weaker inside the cilium of AWC neurons compared to animals co-expressing
456 VC::UNC-119 and ODR-3^{WT}::VN (Supplementary Fig. 7a). These results are consistent with the

457 hypothesis that ciliary transport of the ODR-3-UNC-119 complex may be compromised by the
458 *A328P* mutation – a finding that is consistent with accumulation of the endogenously tagged
459 ODR-3^{A328P}::split-wrmScarlet at cilia base (see Supplementary Fig. 3).

460 **The *T48I*, *K272R*, and *A328P* variants in the guanine-binding domains and *V334E* variant**
461 **in the putative receptor-binding motif impair AWC-mediated chemotaxis**

462 We next examined the impact of orthologous variants on sensory responses mediated
463 by AWC. Ciliated endings of AWC neurons are enveloped in the glial processes (Doroquez et
464 al., 2014; Perkins et al., 1986) and house signaling machinery that detects a panel of volatile
465 attractants including benzaldehyde (Bargmann et al., 1993; Ferkey et al., 2021). However, prior
466 studies reported that these primary behavioral responses to volatile odorants are preserved in
467 several mutants with severely compromised cilia morphology (Campagna et al., 2023; Philbrook
468 et al., 2024), thereby uncoupling cilia morphology from cilia function in mediating odorant
469 sensing by AWC. To investigate the impact of orthologous patient variants on ODR-3-
470 dependent attraction toward benzaldehyde, we carried out population chemotaxis assays (Fig.
471 5c). As expected, wild-type animals exhibited robust attraction to benzaldehyde (1:200), while
472 *odr-3(lf)* animals were deficient in this response (Roayaie et al., 1998) (Fig. 5d). *M88V* and
473 *I321T* mutants exhibited normal chemotaxis, suggesting that these variants do not impair ODR-
474 3 function in either AWC ciliogenesis or chemotaxis toward benzaldehyde. On the other hand,
475 *D175V* mutants exhibited normal behavioral response (Fig. 5d), despite having morphologically
476 defective AWC cilia (see Fig. 5a and b). Normal chemotaxis of *D175V* mutants was particularly
477 intriguing given the dramatic impact of this variant on ciliary localization of the encoded ODR-3
478 protein (see Fig. 3a) and suggests that ODR-3 enrichment inside the AWC cilium may be
479 important for its role in mediating ciliogenesis but not benzaldehyde attraction.

480 The variants mapping to the nucleotide-binding domain all resulted in impaired
481 chemotaxis toward benzaldehyde. Specifically, *A328P* and *T48I* homozygous mutants as well

482 as transgenic animals expressing *odr-3*^{K272R} cDNA in *odr-3(lf)* AWC neurons exhibited
483 significantly lower chemotaxis indices compared to wild type (Fig. 5d and e), consistent with the
484 hypothesis that these variants disrupt overall ODR-3 function. Of note, the *V334E* variant, which
485 alters an amino acid in the putative GPCR-interaction motif, also negatively impacted ODR-3-
486 mediated behavior (Fig. 5d), suggesting that this missense mutation may disrupt ODR-3
487 association with GPCRs. The summary of all cellular and behavioral phenotypes exhibited by
488 the orthologous patient variants is provided in Table 1.

489 **The *D175V* variant disrupts ODR-3 ciliary localization and sensory function of ASH**
490 **neurons**

491 In addition to AWC, *odr-3* is expressed in several sensory neurons including the
492 nociceptor ASH that detects a range of aversive chemicals (Roayaie et al., 1998). Similarly to
493 AWC, *odr-3* mediates chemosensory transduction in ASH neurons (Bargmann et al., 1993;
494 Roayaie et al., 1998; Yoshida et al., 2012). However, *odr-3* function appears to be dispensable
495 for ASH cilium assembly (Roayaie et al., 1998) (Supplementary Fig. 8), pointing to cell-specific
496 roles for this gene in cilia biology.

497 Unlike AWC, ASH neurons possess simple rod-like cilia that extend through a glial
498 channel and are exposed to the external environment (Doroquez et al., 2014; Perkins et al.,
499 1986) (Fig. 6a). A recent study demonstrated that a minimum ASH cilium length is required for
500 ASH-mediated sensory responses to aqueous chemicals, including behavioral avoidance of
501 high-osmolarity solutions (Philbrook et al., 2024). In this context, the minimum length is likely
502 necessary to allow for direct contact between aqueous cues and cilia-localized signaling
503 machinery. Therefore, we wondered whether the *D175V* variant, which excludes the encoded
504 ODR-3 protein from the cilium but does not impair chemotaxis in AWC neurons, may have a
505 different effect on the ASH cilium function. First, we confirmed that TagRFP-tagged ODR-3^{WT}
506 expressed under the *sra-6* regulatory sequences localized to ASH cilia in wild-type animals (Fig.

507 6b). Like in AWC, ODR-3^{D175V} expressed in ASH neurons of wild type *C. elegans* was largely
508 excluded from cilia and instead accumulated in the distal dendrite (Fig. 6b and c), suggesting
509 that *D175V* mutation interferes with ODR-3 trafficking mechanisms conserved across cell types.

510 Next, we examined whether ODR-3 localization to the ASH cilium is required for its
511 function in mediating avoidance of high-osmolarity solutions. To this end, we placed wild-type,
512 *odr-3(lf)*, or *D175V* homozygous animals inside a ring of 8M glycerol and counted the number of
513 animals that escaped the glycerol ring within two minutes (Cornils et al., 2016) (Fig. 6d). On
514 average, 80% of wild-type animals avoided glycerol and stayed inside the ring (Fig. 6e). In
515 contrast, *odr-3(lf)* mutants escaped the ring, and only 40% of *odr-3(lf)* animals remained inside
516 the ring after two minutes (Fig. 6e). Similarly to *odr-3(lf)* animals, 42% of *D175V* mutants
517 remained inside the glycerol ring after 2 minutes (Fig. 6e), indicating that *D175V* variant impairs
518 ASH sensory function. Importantly, over-expression of wild-type *odr-3* cDNA in ASH neurons of
519 *D175V* animals partially but significantly rescued glycerol avoidance (Fig. 6e), confirming that
520 the observed sensory deficit is not due to a second-site mutation.

521 **D173V, K270R, and A326P patient variants impair ciliary localization of Gαi1 protein in**
522 **human cells**

523 We next explored whether the variants with the strongest impact on ODR-3 localization
524 demonstrated similar localization defects in human cells. Gαi1 was previously reported to
525 localize to primary cilia of cultured mouse fibroblasts (Singh et al., 2015). We first examined
526 sub-cellular localization of wild-type human Gαi1 by transfecting HEK293T cells with *eGFP*-
527 tagged *GNAI1* cDNA. In line with the published data, human Gαi1^{WT}::eGFP was present inside
528 the cilia as well as at the plasma membrane and Golgi (Gabay et al., 2011) (Fig. 7a and b).
529 Strikingly, *D173V*, *K270R*, and *A326P* patient variants orthologous to the examined ODR-3
530 mutants significantly reduced intra-ciliary levels of the encoded proteins relative to Golgi (Fig. 7a

531 and b), demonstrating that the impact of these variants on Gα protein trafficking is evolutionarily
532 conserved.

533 **DISCUSSION**

534 **Orthologous *GNAI1*-disorder patient variants differentially impact *odr-3* function.**

535 Here, we demonstrate that *GNAI1* – the causal gene in a recently identified
536 neurodevelopmental disorder – regulates ciliogenesis in two human cell lines, suggesting that
537 cilia dysfunction may play a role in the pathogenesis of *GNAI1* disorder. We used *C. elegans* as
538 a whole-animal model to functionally classify a subset of orthologous *GNAI1* disorder mutations
539 *in vivo* and found variant- and cell-specific effects on the examined phenotypes. Overall,
540 orthologous missense mutations that altered conserved amino-acid residues in the nucleotide-
541 binding interface of Gα (ODR-3: *T48I*, *K272R*, and *A328P*) caused defects in both examined
542 ODR-3-dependent phenotypes – AWC cilia morphology and chemotaxis behavior. Similarly, the
543 *V334E* variant, which maps to the terminal α5 helix of Gα ODR-3, caused a mild reduction in
544 AWC cilia size and significantly impaired attraction to benzaldehyde. The α5 helix of Gα
545 proteins participates in GPCR binding and receptor-catalyzed nucleotide exchange (Alexander
546 et al., 2014; Marin et al., 2002; Masuho et al., 2023; Oldham et al., 2006). Furthermore, the
547 *V332A* substitution was shown to significantly destabilized the GDP-bound state of Gαi1 (Sun et
548 al., 2015). Therefore, additional *in vitro* studies could shed more light on GPCR binding
549 efficiency and nucleotide exchange rates of *V332E* Gαi1 variant present in *GNAI1* disorder
550 patients.

551 On the other hand, variants altering conserved amino acids in domains of unknown
552 function (ODR-3: *M88V* and *I321T*) had no impact on either AWC cilia morphology or behavior.
553 Recent studies have begun to highlight challenges associated with interpreting pathogenicity of
554 *de novo* variants across developmental disorders (Mani, 2017). For example, one study

555 estimated that only ~13% of *de novo* missense variants contribute to risk of autism-spectrum
556 disorder (Iossifov et al., 2014). Therefore, functional studies in additional *in vivo* models are
557 needed to confirm the potentially benign or disease-contributing nature of *M88V* and *I321T*
558 variants.

559 Intriguingly, the *D175V* variant, which caused marked mislocalization of the encoded
560 ODR-3 protein from the cilium to the distal dendrite, was associated with significantly reduced
561 AWC cilia size, yet had no impact on AWC-mediated attraction to benzaldehyde. In stark
562 contrast, the same *D175V* variant did not affect cilia length in ASH neurons but compromised
563 ASH-mediated glycerol avoidance, demonstrating that the functional impact of the same variant
564 varies depending on the cellular context. Context-dependent differences in functional effects of
565 patient variants have also been reported for other disorders (Di Rocco et al., 2023; Feng et al.,
566 2017; Muntean et al., 2021; Wang et al., 2022; Wong et al., 2019), highlighting the importance
567 of modeling patient mutations in multiple experimental systems and disease-relevant contexts to
568 gain a comprehensive understanding of the underlying disease mechanisms.

569 **Modeling orthologous *GNAI1*-disorder missense variants in *C. elegans* provides**
570 **additional insight into cell-specific functions of ODR-3.**

571 Three of the examined orthologous variants (ODR-3: *D175V*, *K272R*, and *A328P*)
572 caused qualitatively and quantitatively similar defects in localization of the encoded ODR-3
573 proteins. Specifically, mutant ODR-3 variants accumulated in the distal dendrite and were
574 present at markedly reduced levels inside the AWC cilium, where wild-type ODR-3 normally
575 resides. Both *K272R* and *A328P* variants alter amino acids that come into direct contact with the
576 nucleotide. Although the *D175* residue does not directly bind GDP, it is found in the immediate
577 vicinity of the nucleotide-binding motif (see Fig. 2) (Kant et al., 2016). Prior *in vitro* work showed
578 that a different missense mutation at the A326 position of Gαi1 (*A326S*) accelerated
579 dissociation of GDP from the αi1β1γ1 heterotrimer by > 200-fold (Posner et al., 1998),

580 suggesting that proper confirmation of the nucleotide-binding pocket or GDP binding itself may
581 be necessary for efficient translocation of ODR-3/Gαi1 into the cilium. Improved targeting of
582 ODR-3^{A328P} protein to the cilia in *mks-5(lf)* mutants is consistent with the hypothesis that *A328P*
583 mutation impedes translocation of ODR-3 across the TZ. However, based on the results from
584 the BiFC assay, ODR-3^{A328P} appears to still interact with UNC-119 – a key mediator of Gα ciliary
585 transport – suggesting that additional mechanisms may contribute to Gα trafficking into the
586 cilium. Since the BiFC signal is binary (either on or off), in the future, it would be worthwhile to
587 directly examine the stability of UNC-119 complexes with ODR-3/Gαi1 proteins carrying
588 *D175V/D173V*, *K272R/K270R*, and *A328P/A326P* patient substitutions using biochemical
589 approaches.

590 We also found that although the *D175V* variant caused mislocalization of the encoded
591 ODR-3 protein from the cilium to the dendrite, it did not alter chemotaxis toward benzaldehyde.
592 This observation led us to conclude that ODR-3 localization to the cilium is not necessary for its
593 function in mediating primary behavioral responses to volatile odorants detected by AWC.
594 Similarly, a recent study demonstrated that diacetyl receptor ODR-10 and Gα ODR-3, which
595 also functions downstream from ODR-10 to mediate attraction toward diacetyl, translocate from
596 the cilium to dendritic branches in AWA olfactory neurons upon disruption of intraflagellar
597 transport (IFT) (Philbrook et al., 2024). Interestingly, IFT mutants retain normal primary
598 responses to diacetyl but exhibit defects in habituation and desensitization (Larsch et al., 2015;
599 Philbrook et al., 2024). It will be of interest to determine whether sequestration of ODR-3^{D175V} in
600 the distal dendrite similarly impacts desensitization and habituation responses of AWA and
601 AWC sensory neurons.

602 Finally, in contrast to AWC, ODR-3 localization to the ASH cilium is required for its
603 function in glycerol avoidance, as *D175V* homozygous mutants exhibit marked deficits in this
604 ASH-mediated sensory behavior despite having cilia of normal length. Recent electron

605 microscopy studies in the human and mouse cortex uncovered remarkable complexity of cilia
606 interactions with the cellular environment in the brain (Ott et al., 2024; Wu et al., 2024).
607 Neuronal cilia were shown to be immersed into dense neuropil and adjacent to axonal and
608 dendritic processes at several points along their length (Ott et al., 2024). Occasionally, tips of
609 neuronal cilia were also found to be enveloped by astrocytes. While the exact nature and
610 functional significance of these interactions remain a mystery, synapses were frequently
611 observed adjacent to cilia in mouse and human cortical tissue (Ott et al., 2024; Wu et al., 2024),
612 and one study even reported axo-ciliary synapses between brainstem axons and cilia of
613 hippocampal CA1 neurons (Sheu et al., 2022). Collectively, these observations propose an
614 exciting hypothesis that primary cilia may be a major player in neural circuit modulation.
615 Therefore, mislocalization of Gαi1 – a key transducer of GPCR signaling that modulates many
616 aspects of neuronal physiology – from cilia to ectopic sub-cellular locations may have a sizeable
617 impact on local neural connectivity as well as neuron-neuron and/or neuron-glia communication.
618 It would be worthwhile to determine whether the patient Gαi1 variants that exhibit reduced ciliary
619 levels in *C. elegans* neurons and human epithelial cells are similarly excluded from cilia of
620 distinct neuron classes in the mammalian brain and to classify their impact on neuronal cilia
621 length and circuit function.

622 In conclusion, our results highlight the power of *C. elegans* as a whole-organism system
623 to rapidly determine functional impact of missense patient variants in conserved Gα residues
624 and thus prioritize functionally consequential mutations for further mechanistic studies in
625 mammalian models and/or additional disease-relevant contexts. Moreover, orthologous
626 disease-associated mutations in model organisms like *C. elegans* can provide new insights into
627 normal function of the impacted genes.

628 **Data availability**

629 Strains and plasmids used in this work are listed in Supplementary Tables 1 and 2,
630 respectively, and are available upon request. All data necessary for confirming the conclusions
631 of the article are present within the article, figures, table, and supplementary files.

632 **Acknowledgements**

633 We are grateful to members of the Nechipurenko lab for critical comments on the
634 manuscript and to Ryan Breitenbach for technical assistance and maintenance of strains. Some
635 strains were provided by the CGC, which is funded by NIH Office of Research Infrastructure
636 Programs (P40 OD010440).

637 **Study funding**

638 This work was supported by the Charles H. Hood Foundation [Child Health Research
639 Award to I.N.] and in part by the National Institutes of Health [R35 GM155316 to I.N.].

640 **Conflicts of interest**

641 The authors declare no conflicts of interest.

642 **REFERENCES**

643 Alexander, N. S., Preininger, A. M., Kaya, A. I., Stein, R. A., Hamm, H. E., & Meiler, J. (2014).
644 Energetic analysis of the rhodopsin-G-protein complex links the alpha5 helix to GDP
645 release. *Nat Struct Mol Biol*, *21*(1), 56-63. https://doi.org/10.1038/nsmb.2705
646 Algar, W. R., Hildebrandt, N., Vogel, S. S., & Medintz, I. L. (2019). FRET as a biomolecular
647 research tool — understanding its potential while avoiding pitfalls. *Nature Methods*,
648 *16*(9), 815-829. https://doi.org/10.1038/s41592-019-0530-8
649 Anvarian, Z., Mykytyn, K., Mukhopadhyay, S., Pedersen, L. B., & Christensen, S. T. (2019).
650 Cellular signalling by primary cilia in development, organ function and disease.
651 *Nature Reviews Nephrology*, *15*(4), 199-219. https://doi.org/10.1038/s41581-019-
652 0116-9
653 Bargmann, C. I., Hartwieg, E., & Horvitz, H. R. (1993). Odorant-selective genes and neurons
654 mediate olfaction in C. elegans. *Cell*, *74*(3), 515-527. https://doi.org/10.1016/0092-
655 8674(93)80053-h

656 Betke, K. M., Wells, C. A., & Hamm, H. E. (2012). GPCR mediated regulation of synaptic
657 transmission. *Prog Neurobiol*, *96*(3), 304-321.
658 https://doi.org/10.1016/j.pneurobio.2012.01.009
659 Brenner, S. (1974). The genetics of Caenorhabditis elegans. *Genetics*, *77*(1), 71-94.
660 https://doi.org/10.1093/genetics/77.1.71
661 Campagna, C. M., McMahon, H., & Nechipurenko, I. (2023). The G protein alpha chaperone
662 and guanine-nucleotide exchange factor RIC-8 regulates cilia morphogenesis in
663 Caenorhabditis elegans sensory neurons. *PLoS Genetics*, *19*(11), e1011015.
664 https://doi.org/10.1371/journal.pgen.1011015
665 Cevik, S., Sanders, A. A., Van Wijk, E., Boldt, K., Clarke, L., van Reeuwijk, J., Hori, Y., Horn,
666 N., Hetterschijt, L., Wdowicz, A., Mullins, A., Kida, K., Kaplan, O. I., van Beersum, S.
667 E., Man Wu, K., Letteboer, S. J., Mans, D. A., Katada, T., Kontani, K., . . . Blacque, O.
668 E. (2013). Active transport and diffusion barriers restrict Joubert Syndrome-
669 associated ARL13B/ARL-13 to an Inv-like ciliary membrane subdomain. *PLoS*
670 *Genet*, *9*(12), e1003977. https://doi.org/10.1371/journal.pgen.1003977
671 Cornils, A., Maurya, A. K., Tereshko, L., Kennedy, J., Brear, A. G., Prahlad, V., Blacque, O.
672 E., & Sengupta, P. (2016). Structural and Functional Recovery of Sensory Cilia in C.
673 elegans IFT Mutants upon Aging. *PLoS Genetics*, *12*(12), e1006325.
674 https://doi.org/10.1371/journal.pgen.1006325
675 Culotti, J. G., & Russell, R. L. (1978). Osmotic avoidance defective mutants of the
676 nematode Caenorhabditis elegans. *Genetics*, *90*(2), 243-256.
677 https://doi.org/10.1093/genetics/90.2.243
678 Di Rocco, M., Galosi, S., Follo, F. C., Lanza, E., Folli, V., Martire, A., Leuzzi, V., & Martinelli,
679 S. (2023). Phenotypic Assessment of Pathogenic Variants in GNAO1 and Response
680 to Caffeine in C. elegans Models of the Disease. *Genes (Basel)*, *14*(2).
681 https://doi.org/10.3390/genes14020319
682 Dokshin, G. A., Ghanta, K. S., Piscopo, K. M., & Mello, C. C. (2018). Robust Genome Editing
683 with Short Single-Stranded and Long, Partially Single-Stranded DNA Donors in
684 Caenorhabditis elegans. *Genetics*, *210*(3), 781-787.
685 https://doi.org/10.1534/genetics.118.301532
686 Doroquez, D. B., Berciu, C., Anderson, J. R., Sengupta, P., & Nicastro, D. (2014). A high-
687 resolution morphological and ultrastructural map of anterior sensory cilia and glia
688 in Caenorhabditis elegans. *eLife*, *3*. https://doi.org/10.7554/elife.01948
689 Dror, R. O., Mildorf, T. J., Hilger, D., Manglik, A., Borhani, D. W., Arlow, D. H., Philippsen, A.,
690 Villanueva, N., Yang, Z., Lerch, M. T., Hubbell, W. L., Kobilka, B. K., Sunahara, R. K.,
691 & Shaw, D. E. (2015). SIGNAL TRANSDUCTION. Structural basis for nucleotide
692 exchange in heterotrimeric G proteins. *Science*, *348*(6241), 1361-1365.
693 https://doi.org/10.1126/science.aaa5264
694 Feng, H., Sjögren, B., Karaj, B., Shaw, V., Gezer, A., & Neubig, R. R. (2017). Movement
695 disorder in GNAO1 encephalopathy associated with gain-of-function mutations.
696 *Neurology*, *89*(8), 762-770. https://doi.org/10.1212/wnl.0000000000004262
697 Ferkey, D. M., Sengupta, P., & L'Etoile, N. D. (2021). Chemosensory signal transduction in
698 Caenorhabditis elegans. *Genetics*, *217*(3).
699 https://doi.org/10.1093/genetics/iyab004

Gabay, M., Pinter, M. E., Wright, F. A., Chan, P., Murphy, A. J., Valenzuela, D. M., Yancopoulos, G. D., & Tall, G. G. (2011). Ric-8 Proteins Are Molecular Chaperones That Direct Nascent G Protein Subunit Membrane Association. *Science Signaling*, *4*(200), ra79-ra79. https://doi.org/10.1126/scisignal.2002223

Garcia-Gonzalo, F. R., & Reiter, J. F. (2017). Open Sesame: How Transition Fibers and the Transition Zone Control Ciliary Composition. *Cold Spring Harbor Perspectives in Biology*, *9*(2), a028134. https://doi.org/10.1101/cshperspect.a028134

Gilman, A. G. (1987). G PROTEINS: TRANSDUCERS OF RECEPTOR-GENERATED SIGNALS. *Annual Review of Biochemistry*, *56*(1), 615-649. https://doi.org/10.1146/annurev.bi.56.070187.003151

Goudeau, J., Sharp, C. S., Paw, J., Savy, L., Leonetti, M. D., York, A. G., Updike, D. L., Kenyon, C., & Ingaramo, M. (2021). Split-wrmScarlet and split-sfGFP: tools for faster, easier fluorescent labeling of endogenous proteins in Caenorhabditis elegans. *Genetics*, *217*(4). https://doi.org/10.1093/genetics/iyab014

Guemez-Gamboa, A., Coufal, N. G., & Gleeson, J. G. (2014). Primary cilia in the developing and mature brain. *Neuron*, *82*(3), 511-521. https://doi.org/10.1016/j.neuron.2014.04.024

Hamada, N., Iwamoto, I., Kawamura, N., & Nagata, K. I. (2021). Heterotrimeric G-protein, Gi1, is involved in the regulation of proliferation, neuronal migration, and dendrite morphology during cortical development in vivo. *J Neurochem*, *157*(4), 1167-1181. https://doi.org/10.1111/jnc.15205

Hasenpusch-Theil, K., & Theil, T. (2021). The Multifaceted Roles of Primary Cilia in the Development of the Cerebral Cortex. *Front Cell Dev Biol*, *9*, 630161. https://doi.org/10.3389/fcell.2021.630161

Hildebrandt, F., Benzing, T., & Katsanis, N. (2011). Ciliopathies. *N Engl J Med*, *364*(16), 1533-1543. https://doi.org/10.1056/NEJMra1010172

Hilgendorf, K. I., Johnson, C. T., & Jackson, P. K. (2016). The primary cilium as a cellular receiver: organizing ciliary GPCR signaling. *Current Opinion in Cell Biology*, *39*, 84-92. https://doi.org/10.1016/j.ceb.2016.02.008

Iossifov, I., O'Roak, B. J., Sanders, S. J., Ronemus, M., Krumm, N., Levy, D., Stessman, H. A., Witherspoon, K. T., Vives, L., Patterson, K. E., Smith, J. D., Paeper, B., Nickerson, D. A., Dea, J., Dong, S., Gonzalez, L. E., Mandell, J. D., Mane, S. M., Murtha, M. T., . . . Wigler, M. (2014). The contribution of de novo coding mutations to autism spectrum disorder. *Nature*, *515*(7526), 216-221. https://doi.org/10.1038/nature13908

Jensen, V. L., Li, C., Bowie, R. V., Clarke, L., Mohan, S., Blacque, O. E., & Leroux, M. R. (2015). Formation of the transition zone by Mks5/Rpgrip1L establishes a ciliary zone of exclusion (CIZE) that compartmentalises ciliary signalling proteins and controls PIP2 ciliary abundance. *The EMBO Journal*, *34*(20), 2537-2556. https://doi.org/10.15252/embj.201488044

Jurisch-Yaksi, N., Wachten, D., & Gopalakrishnan, J. (2024). The neuronal cilium - a highly diverse and dynamic organelle involved in sensory detection and neuromodulation. *Trends Neurosci*, *47*(5), 383-394. https://doi.org/10.1016/j.tins.2024.03.004

742 Kant, R., Zeng, B., Thomas, C. J., Bothner, B., & Sprang, S. R. (2016). Ric-8A, a G protein
743 chaperone with nucleotide exchange activity induces long-range secondary
744 structure changes in Gα. *eLife*, *5*. https://doi.org/10.7554/elife.19238
745 Karalis, V., Donovan, K. E., & Sahin, M. (2022). Primary Cilia Dysfunction in
746 Neurodevelopmental Disorders beyond Ciliopathies. *J Dev Biol*, *10*(4).
747 https://doi.org/10.3390/jdb10040054
748 Kerppola, T. K. (2008). Bimolecular Fluorescence Complementation (BiFC) Analysis as a
749 Probe of Protein Interactions in Living Cells. *Annual Review of Biophysics*, *37*(1),
750 465-487. https://doi.org/10.1146/annurev.biophys.37.032807.125842
751 Kim, K., Kim, R., & Sengupta, P. (2010). The HMX/NKX homeodomain protein MLS-2
752 specifies the identity of the AWC sensory neuron type via regulation of the ceh-36
753 Otx gene in C. elegans. *Development*, *137*(6), 963-974.
754 https://doi.org/10.1242/dev.044719
755 Kurabayashi, N., Nguyen, M. D., & Sanada, K. (2013). The G protein-coupled receptor
756 GPRC5B contributes to neurogenesis in the developing mouse neocortex.
757 *Development*, *140*(21), 4335-4346. https://doi.org/10.1242/dev.099754
758 Lange, K. I., Best, S., Tsiropoulou, S., Berry, I., Johnson, C. A., & Blacque, O. E. (2022).
759 Interpreting ciliopathy-associated missense variants of uncertain significance (VUS)
760 in Caenorhabditis elegans. *Hum Mol Genet*, *31*(10), 1574-1587.
761 https://doi.org/10.1093/hmg/ddab344
762 Lange, K. I., Tsiropoulou, S., Kucharska, K., & Blacque, O. E. (2021). Interpreting the
763 pathogenicity of Joubert syndrome missense variants in Caenorhabditis elegans.
764 *Dis Model Mech*, *14*(1). https://doi.org/10.1242/dmm.046631
765 Lans, H., Rademakers, S., & Jansen, G. (2004). A Network of Stimulatory and Inhibitory Gα-
766 Subunits Regulates Olfaction in Caenorhabditis elegans. *Genetics*, *167*(4), 1677-
767 1687. https://doi.org/10.1534/genetics.103.024786
768 Larsch, J., Flavell, S. W., Liu, Q., Gordus, A., Albrecht, D. R., & Bargmann, C. I. (2015). A
769 Circuit for Gradient Climbing in C. elegans Chemotaxis. *Cell Rep*, *12*(11), 1748-
770 1760. https://doi.org/10.1016/j.celrep.2015.08.032
771 Lee, J. E., & Gleeson, J. G. (2011). Cilia in the nervous system: linking cilia function and
772 neurodevelopmental disorders. *Curr Opin Neurol*, *24*(2), 98-105.
773 https://doi.org/10.1097/WCO.0b013e3283444d05
774 Luo, M., Han, Z., Huang, G., Li, R., Liu, Y., Lu, J., Liu, L., & Miao, R. (2022). Structural
775 comparison of unconventional G protein YchF with heterotrimeric G protein and
776 small G protein. *Plant Signal Behav*, *17*(1), 2024405.
777 https://doi.org/10.1080/15592324.2021.2024405
778 Mani, A. (2017). Pathogenicity of De Novo Rare Variants: Challenges and Opportunities.
779 *Circ Cardiovasc Genet*, *10*(6). https://doi.org/10.1161/CIRCGENETICS.117.002013
780 Marin, E. P., Krishna, A. G., & Sakmar, T. P. (2002). Disruption of the alpha5 helix of
781 transducin impairs rhodopsin-catalyzed nucleotide exchange. *Biochemistry*,
782 *41*(22), 6988-6994. https://doi.org/10.1021/bi025514k
783 Masuho, I., Kise, R., Gainza, P., Von Moo, E., Li, X., Tany, R., Wakasugi-Masuho, H.,
784 Correia, B. E., & Martemyanov, K. A. (2023). Rules and mechanisms governing G

785 protein coupling selectivity of GPCRs. *Cell Rep*, *42*(10), 113173.
786 https://doi.org/10.1016/j.celrep.2023.113173
787 Muir, A. M., Gardner, J. F., Van Jaarsveld, R. H., De Lange, I. M., Van Der Smagt, J. J.,
788 Wilson, G. N., Dubbs, H., Goldberg, E. M., Zitano, L., Bupp, C., Martinez, J., Srour,
789 M., Accogli, A., Alhakeem, A., Meltzer, M., Gropman, A., Brewer, C., Caswell, R. C.,
790 Montgomery, T., . . . Mefford, H. C. (2021). Variants in GNAI1 cause a syndrome
791 associated with variable features including developmental delay, seizures, and
792 hypotonia. *Genetics in Medicine*, *23*(5), 881-887. https://doi.org/10.1038/s41436-
793 020-01076-8
794 Muntean, B. S., Masuho, I., Dao, M., Sutton, L. P., Zucca, S., Iwamoto, H., Patil, D. N.,
795 Wang, D., Birnbaumer, L., Blakely, R. D., Grill, B., & Martemyanov, K. A. (2021). Gαo
796 is a major determinant of cAMP signaling in the pathophysiology of movement
797 disorders. *Cell Reports*, *34*(5), 108718.
798 https://doi.org/10.1016/j.celrep.2021.108718
799 Nechipurenko, I. V., Olivier-Mason, A., Kazatskaya, A., Kennedy, J., McLachlan, I. G.,
800 Heiman, M. G., Blacque, O. E., & Sengupta, P. (2016). A Conserved Role for Girdin in
801 Basal Body Positioning and Ciliogenesis. *Dev Cell*, *38*(5), 493-506.
802 https://doi.org/10.1016/j.devcel.2016.07.013
803 Noel, J. P., Hamm, H. E., & Sigler, P. B. (1993). The 2.2 A crystal structure of transducin-
804 alpha complexed with GTP gamma S. *Nature*, *366*(6456), 654-663.
805 https://doi.org/10.1038/366654a0
806 Oldham, W. M., Van Eps, N., Preininger, A. M., Hubbell, W. L., & Hamm, H. E. (2006).
807 Mechanism of the receptor-catalyzed activation of heterotrimeric G proteins. *Nat*
808 *Struct Mol Biol*, *13*(9), 772-777. https://doi.org/10.1038/nsmb1129
809 Ott, C. M., Torres, R., Kuan, T. S., Kuan, A., Buchanan, J., Elabbady, L., Seshamani, S.,
810 Bodor, A. L., Collman, F., Bock, D. D., Lee, W. C., da Costa, N. M., & Lippincott-
811 Schwartz, J. (2024). Ultrastructural differences impact cilia shape and external
812 exposure across cell classes in the visual cortex. *Curr Biol*, *34*(11), 2418-2433
813 e2414. https://doi.org/10.1016/j.cub.2024.04.043
814 Perkins, L. A., Hedgecock, E. M., Thomson, J. N., & Culotti, J. G. (1986). Mutant sensory
815 cilia in the nematode Caenorhabditis elegans. *Dev Biol*, *117*(2), 456-487.
816 https://doi.org/10.1016/0012-1606(86)90314-3
817 Philbrook, A., O'Donnell, M. P., Grunenkovaite, L., & Sengupta, P. (2024). Cilia structure
818 and intraflagellar transport differentially regulate sensory response dynamics within
819 and between C. elegans chemosensory neurons. *PLOS Biology*, *22*(11), e3002892.
820 https://doi.org/10.1371/journal.pbio.3002892
821 Pierce, K. L., Premont, R. T., & Lefkowitz, R. J. (2002). Seven-transmembrane receptors. *Nat*
822 *Rev Mol Cell Biol*, *3*(9), 639-650. https://doi.org/10.1038/nrm908
823 Pineda, V. V., Athos, J. I., Wang, H., Celver, J., Ippolito, D., Boulay, G., Birnbaumer, L., &
824 Storm, D. R. (2004). Removal of G(ialpha1) constraints on adenylyl cyclase in the
825 hippocampus enhances LTP and impairs memory formation. *Neuron*, *41*(1), 153-
826 163. https://doi.org/10.1016/s0896-6273(03)00813-4

827 Posner, B. A., Mixon, M. B., Wall, M. A., Sprang, S. R., & Gilman, A. G. (1998). The A326S
828 mutant of Gialpha1 as an approximation of the receptor-bound state. *J Biol Chem*,
829 *273*(34), 21752-21758. https://doi.org/10.1074/jbc.273.34.21752
830 Reiter, J. F., & Leroux, M. R. (2017). Genes and molecular pathways underpinning
831 ciliopathies. *Nature Reviews Molecular Cell Biology*, *18*(9), 533-547.
832 https://doi.org/10.1038/nrm.2017.60
833 Roayaie, K., Crump, J. G., Sagasti, A., & Bargmann, C. I. (1998). The Gα Protein ODR-3
834 Mediates Olfactory and Nociceptive Function and Controls Cilium Morphogenesis
835 in C. elegans Olfactory Neurons. *Neuron*, *20*(1), 55-67.
836 https://doi.org/10.1016/s0896-6273(00)80434-1
837 Seven, A. B., Hilger, D., Papasergi-Scott, M. M., Zhang, L., Qu, Q., Kobilka, B. K., Tall, G. G.,
838 & Skiniotis, G. (2020). Structures of Gα Proteins in Complex with Their Chaperone
839 Reveal Quality Control Mechanisms. *Cell Reports*, *30*(11), 3699-3709.e3696.
840 https://doi.org/10.1016/j.celrep.2020.02.086
841 Sheu, S. H., Upadhyayula, S., Dupuy, V., Pang, S., Deng, F., Wan, J., Walpita, D., Pasolli, H.
842 A., Houser, J., Sanchez-Martinez, S., Brauchi, S. E., Banala, S., Freeman, M., Xu, C.
843 S., Kirchhausen, T., Hess, H. F., Lavis, L., Li, Y., Chaumont-Dubel, S., & Clapham, D.
844 E. (2022). A serotonergic axon-cilium synapse drives nuclear signaling to alter
845 chromatin accessibility. *Cell*, *185*(18), 3390-3407 e3318.
846 https://doi.org/10.1016/j.cell.2022.07.026
847 Shyu, Y. J., Hiatt, S. M., Duren, H. M., Ellis, R. E., Kerppola, T. K., & Hu, C.-D. (2008).
848 Visualization of protein interactions in living Caenorhabditis elegans using
849 bimolecular fluorescence complementation analysis. *Nature Protocols*, *3*(4), 588-
850 596. https://doi.org/10.1038/nprot.2008.16
851 Singh, J., Wen, X., & Scales, S. J. (2015). The Orphan G Protein-coupled Receptor Gpr175
852 (Tpra40) Enhances Hedgehog Signaling by Modulating cAMP Levels. *J Biol Chem*,
853 *290*(49), 29663-29675. https://doi.org/10.1074/jbc.M115.665810
854 Sprang, S. R. (1997). G protein mechanisms: insights from structural analysis. *Annu Rev*
855 *Biochem*, *66*, 639-678. https://doi.org/10.1146/annurev.biochem.66.1.639
856 Stoufflet, J., & Caille, I. (2022). The Primary Cilium and Neuronal Migration. *Cells*, *11*(21).
857 https://doi.org/10.3390/cells11213384
858 Suciu, S. K., & Caspary, T. (2021). Cilia, neural development and disease. *Semin Cell Dev*
859 *Biol*, *110*, 34-42. https://doi.org/10.1016/j.semcdb.2020.07.014
860 Sun, D., Flock, T., Deupi, X., Maeda, S., Matkovic, M., Mendieta, S., Mayer, D., Dawson, R.,
861 Schertler, G. F. X., Madan Babu, M., & Veprintsev, D. B. (2015). Probing Galphai1
862 protein activation at single-amino acid resolution. *Nat Struct Mol Biol*, *22*(9), 686-
863 694. https://doi.org/10.1038/nsmb.3070
864 Valente, E. M., Rosti, R. O., Gibbs, E., & Gleeson, J. G. (2014). Primary cilia in
865 neurodevelopmental disorders. *Nat Rev Neurol*, *10*(1), 27-36.
866 https://doi.org/10.1038/nrneurol.2013.247
867 Varadi, M., Anyango, S., Deshpande, M., Nair, S., Natassia, C., Yordanova, G., Yuan, D.,
868 Stroe, O., Wood, G., Laydon, A., Zidek, A., Green, T., Tunyasuvunakool, K., Petersen,
869 S., Jumper, J., Clancy, E., Green, R., Vora, A., Lutfi, M., . . . Velankar, S. (2022).
870 AlphaFold Protein Structure Database: massively expanding the structural coverage

of protein-sequence space with high-accuracy models. *Nucleic Acids Res*, *50*(D1), D439-D444. https://doi.org/10.1093/nar/gkab1061

Varadi, M., Bertoni, D., Magana, P., Paramval, U., Pidruchna, I., Radhakrishnan, M., Tsenkov, M., Nair, S., Mirdita, M., Yeo, J., Kovalevskiy, O., Tunyasuvunakool, K., Laydon, A., Zidek, A., Tomlinson, H., Hariharan, D., Abrahamson, J., Green, T., Jumper, J., . . . Velankar, S. (2024). AlphaFold Protein Structure Database in 2024: providing structure coverage for over 214 million protein sequences. *Nucleic Acids Res*, *52*(D1), D368-D375. https://doi.org/10.1093/nar/gkad1011

Wang, D., Dao, M., Muntean, B. S., Giles, A. C., Martemyanov, K. A., & Grill, B. (2022). Genetic modeling of GNAO1 disorder delineates mechanisms of Gαo dysfunction. *Human Molecular Genetics*, *31*(4), 510-522. https://doi.org/10.1093/hmg/ddab235

Wettschureck, N., & Offermanns, S. (2005). Mammalian G proteins and their cell type specific functions. *Physiol Rev*, *85*(4), 1159-1204. https://doi.org/10.1152/physrev.00003.2005

Wong, W. R., Brugman, K. I., Maher, S., Oh, J. Y., Howe, K., Kato, M., & Sternberg, P. W. (2019). Autism-associated missense genetic variants impact locomotion and neurodevelopment in Caenorhabditis elegans. *Hum Mol Genet*, *28*(13), 2271-2281. https://doi.org/10.1093/hmg/ddz051

Wright, K. J., Baye, L. M., Olivier-Mason, A., Mukhopadhyay, S., Sang, L., Kwong, M., Wang, W., Pretorius, P. R., Sheffield, V. C., Sengupta, P., Slusarski, D. C., & Jackson, P. K. (2011). An ARL3-UNC119-RP2 GTPase cycle targets myristoylated NPHP3 to the primary cilium. *Genes Dev*, *25*(22), 2347-2360. https://doi.org/10.1101/gad.173443.111

Wu, J. Y., Cho, S. J., Descant, K., Li, P. H., Shapson-Coe, A., Januszewski, M., Berger, D. R., Meyer, C., Casingal, C., Huda, A., Liu, J., Ghashghaei, T., Brenman, M., Jiang, M., Scarborough, J., Pope, A., Jain, V., Stein, J. L., Guo, J., . . . Anton, E. S. (2024). Mapping of neuronal and glial primary cilia contactome and connectome in the human cerebral cortex. *Neuron*, *112*(1), 41-55 e43. https://doi.org/10.1016/j.neuron.2023.09.032

Xing, S., Wallmeroth, N., Berendzen, K. W., & Grefen, C. (2016). Techniques for the analysis of protein-protein interactions in vivo. *Plant Physiology*, pp.00470.02016. https://doi.org/10.1104/pp.16.00470

Yoshida, K., Hirotsu, T., Tagawa, T., Oda, S., Wakabayashi, T., Iino, Y., & Ishihara, T. (2012). Odour concentration-dependent olfactory preference change in C. elegans. *Nat Commun*, *3*, 739. https://doi.org/10.1038/ncomms1750

Zeng, B., Mou, T.-C., Doukov, T. I., Steiner, A., Yu, W., Papasergi-Scott, M., Tall, G. G., Hagn, F., & Sprang, S. R. (2019). Structure, Function, and Dynamics of the Gα Binding Domain of Ric-8A. *Structure*, *27*(7), 1137-1147.e1135. https://doi.org/10.1016/j.str.2019.04.013

Zhang, H., Constantine, R., Vorobiev, S., Chen, Y., Seetharaman, J., Huang, Y. J., Xiao, R., Montelione, G. T., Gerstner, C. D., Davis, M. W., Inana, G., Whitby, F. G., Jorgensen, E. M., Hill, C. P., Tong, L., & Baehr, W. (2011). UNC119 is required for G protein trafficking in sensory neurons. *Nat Neurosci*, *14*(7), 874-880. https://doi.org/10.1038/nn.2835

915 **FIGURE LEGENDS**

916 **Fig. 1.** *GNAI1* knockdown impairs ciliogenesis in human cells. a – b) Immunofluorescence
917 images of fixed RPE-1 (a) and HEK293T (b) cells transfected with the indicated siRNAs. White
918 arrowheads mark cilia labeled with anti-ARL13B antibody. Scale: 10 μm. c – d) Quantification of
919 ciliation in RPE-1 (c) and HEK293T (d) cells transfected with the indicated siRNAs. Each data
920 point represents one replicate. Total number of cells: siControl (n=858 RPE-1, n=4460
921 HEK293T), si*GNAI1* #1 (n=518 RPE-1, n=4600 HEK293T). Means ± SD are indicated by
922 shaded and vertical bars, respectively. *** indicates different from control at $p<0.001$ (Fisher's
923 exact test). e) Relative levels of *GNAI1* mRNA in RPE-1 and HEK293T cells treated with the
924 indicated siRNAs. Summary data represent > 3 replicates. Error bars are SEM. * indicates
925 different from control at $p<0.05$ (Mann-Whitney test).

926 **Fig. 2.** Distribution of patient variants selected for analysis. a) *Left*: 3D structure of Gαi1 bound
927 to GDP (PDB accession: 2G83). Carbon, oxygen, nitrogen, and phosphorous atoms of GDP are
928 shown in green, red, blue, and orange, respectively. *Right*: AlphaFold-predicted structure of *C.*
929 *elegans* ODR-3 (Varadi et al., 2022; Varadi et al., 2024). Positions of missense patient variants
930 that were selected for analysis are shown in magenta in both protein models. b) Schematic of
931 human Gαi1 showing positions of *GNAI1* disorder-associated variants (green pins). Guanine
932 nucleotide-binding motifs (G1 – G5 boxes) are shown in red.

933 **Fig. 3.** Orthologous patient mutations in the *odr-3* gene differentially affect subcellular
934 localization of the encoded proteins. a) Representative images showing localization of the
935 indicated TagRFP-tagged ODR-3 variants in AWC neurons. AWC neurons were visualized via
936 expression of *ceh-36*p::GFP, which also labels ASE neurons (white arrows). Purple arrowheads
937 mark cilia base. d: dendrite. Anterior is at left. Scale: 5 μm. b) Quantification of relative TagRFP
938 fluorescence inside the AWC cilium vs distal dendrite for the indicated TagRFP-tagged ODR-3

939 variants. Total number of AWC neurons analyzed for each variant: WT (n=27), T48I (n=42),
940 M88V (n=26), D175V (n=22), K272R (n=21), I321T (n=26), A328P (n=28), and V334E (n=29).
941 Means ± SD are indicated by horizontal and vertical bars, respectively. *** indicates different
942 from WT at p<0.001; n.s.: not significant (Kruskal-Wallis with Dunn's multiple comparisons test).

943 **Fig. 4.** Intraciliary localization of A328P ODR-3 variant is increased in *mks-5* mutants. a)
944 Representative images showing localization of TagRFP-tagged ODR-3^{WT} and ODR-3^{A328P}
945 proteins in AWC cilia of wild-type animals (*top*) and *mks-5(tm3100)* mutants (*bottom*). AWC
946 neurons were visualized via expression of *ceh-36*p::GFP, which also labels ASE neurons (white
947 arrows). Purple arrowheads mark cilia base. Anterior is at left. Scale: 5 μm. b) Quantification of
948 relative TagRFP fluorescence inside the AWC cilium vs distal dendrite for the indicated
949 TagRFP-tagged ODR-3 variants in wild-type and *mks-5(tm3100)* mutant animals. Total number
950 of AWC neurons analyzed for each variant: wild type (n=16 ODR-3^{WT}, n=28 ODR-3^{A328P}), *mks-*
951 *5(tm3100)* (n=17 ODR-3^{WT}, n=18 ODR-3^{A328P}). Data for ODR-3^{WT} localization in the wild-type
952 background are repeated from Fig. 3b. Means ± SD are indicated by horizontal and vertical
953 bars, respectively. *** and ### indicate different between bracketed groups at p<0.001; n.s.: not
954 significant (Kruskal-Wallis with Dunn's multiple comparisons test).

955 **Fig. 5.** Orthologous patient mutations in the *odr-3* gene differentially alter AWC cilia morphology
956 and function. a) Representative images of AWC cilia in animals homozygous for the indicated
957 *odr-3* mutations and *odr-3(lf)* animals overexpressing the *odr-3^{K272R}* transgene. AWC neurons
958 were visualized via expression of *ceh-36*p::GFP, which also labels ASE neurons (white arrows).
959 Purple arrowheads mark cilia base. Anterior is at left. Scale: 5 μm. b) Quantification of AWC cilia
960 size in the indicated genotypes. Total number of cilia: WT (n=34), *odr-3(lf)* (n=15), *T48I* (n=31),
961 *M88V* (n=40), *D175V* (n=59), *K272R* (n=45), *I321T* (n=41), *A328P* (n=32), *A328P* rescue
962 (n=32), and *V334E* (n=29). Means ± SD are indicated by shaded and vertical bars, respectively.
963 *, **, and *** indicate different from WT at p<0.05, 0.01, and 0.001, respectively (Kruskal-Wallis

964 with Dunn's multiple comparisons test). ### indicates different between bracketed genotypes at
965 p<0.001 (unpaired t test with Welch's correction); n.s.: not significant (Mann Whitney test). c)
966 Schematic of chemotaxis assay. d) Chemotaxis responses of the indicated homozygous
967 variants. Individual data points represent chemotaxis index from one assay. Total number of
968 assays: WT (n=50), *odr-3(lf)* (n=43), *T48I* (n=8), *M88V* (n=6), *D175V* (n=10), *I321T* (n=4),
969 *A328P* (n=13), *A328P* rescue (n=16), and *V334E* (n=25). Means ± SD are indicated by shaded
970 and vertical bars, respectively. * and *** indicate different from wild type at p<0.05 and 0.001,
971 respectively; n.s.: not significant (Kruskal-Wallis with Dunn's multiple comparisons test). ###
972 indicates different between bracketed genotypes at p<0.001 (unpaired t test with Welch's
973 correction). e) Chemotaxis responses of wild-type, *odr-3(lf)*, and *odr-3(lf)* mutants
974 overexpressing *odr-3*^{K272R} transgene in AWC neurons. Individual data points represent
975 chemotaxis index from one assay. Total number of assays: WT (n=10), *odr-3(lf)* (n=10), and
976 *odr-3(lf)*; *K272* OE (n=10). Means ± SD are indicated by shaded and vertical bars, respectively.
977 ** and *** indicate different from wild type at p<0.01 and 0.001, respectively; n.s.: not significant
978 (Kruskal-Wallis with Dunn's multiple comparisons test).

979 **Fig. 6.** The *D175V* variant disrupts ODR-3 localization to the ASH cilia and impairs ASH-
980 mediated behavior. a) Schematic of the amphid channel. Only AWC and ASH cilia are shown
981 for simplicity. Socket and sheath are glial cells that form the channel. Anterior is up. b)
982 Representative images showing localization of TagRFP-tagged WT and D175V variants of
983 ODR-3 in ASH and ASI neurons. ASH and ASI neurons were visualized via expression of *sra-*
984 *6*p*::*GFP*.* Purple arrowheads mark cilia base. Anterior is at left. Scale: 5 μm. c) Quantification of
985 relative TagRFP fluorescence inside the ASH cilium vs distal dendrite for the indicated TagRFP-
986 tagged ODR-3 variants. Total number of ASH neurons analyzed for each variant: WT (n=32),
987 *D175V* (n=65). *** indicates different from WT at p<0.001 (Mann-Whitney test). d) Diagram of
988 glycerol avoidance assay. e) Fraction of animals that remain inside of an 8M-glycerol ring after

989 two minutes (osmotic avoidance index). Genotypes of assayed animals are indicated. Each data
990 point represents a mean osmotic index per genotype per day. Three to eight technical replicates
991 were assayed per genotype per day. Total number of assayed animals: WT (n=298), *odr-3(lf)*
992 (n=264), *D175V* (n=224), *D175* rescue (n=157). Means ± SD are indicated by shaded and
993 vertical bars, respectively. ** and *** indicate different from wild type at p<0.01 and 0.001,
994 respectively (Fisher's exact test). ### indicates different between bracketed genotypes (Fisher's
995 exact test).

996 **Fig. 7.** The *D173V*, *K270R*, and *A326P* variants in *GNAI1* impair cilia localization of the
997 encoded proteins in human cells. a) Immunofluorescence images of fixed HEK293T cells
998 transfected with the indicated eGFP-tagged Gαi1 variants. White arrowheads mark cilia labeled
999 with anti-ARL13B antibody. DAPI and anti-GOLGA2 label DNA and Golgi, respectively. Scale: 5
1000 μm. b) Quantification of relative eGFP fluorescence in cilium vs Golgi for the indicated eGFP-
1001 tagged Gαi1 variants. Individual biological replicates for each variant are shown in different
1002 shades of the corresponding color. Diamonds: mean of individual biological replicates. Total
1003 mean ± SD across all biological replicates is indicated by horizontal and vertical bars,
1004 respectively. Total number of cells analyzed for each Gαi1 variant: WT (n=322), *D173V* (n=220),
1005 *K270R* (n=260), *A326P* (n=315). *** indicates different from $G\alpha i1^{WT}$ at p<0.001 (Kruskal-Wallis
1006 with Dunn's multiple comparisons test).

1007

1008

1009

1010

1011 **Table 1:** Summary of AWC cellular and behavioral phenotypes caused by orthologous

1012 mutations in the *odr-3* gene.

ODR-3 variant	**T48I**	**M88V**	**D175V**	**K272R**	**I321T**	**A328P**	**V334E**
Functional domain	G box	unknown	G box	G box	unknown	G box	putative GPCR-binding
Encoded variant localization	cilia + PCMC	cilia + PCMC	low inside cilia/ pool at base		wild-type	low inside cilia/ pool at base	wild-type
AWC cilia size	reduced	wild-type	reduced		wild-type	reduced	reduced
Chemotaxis behavior	impaired	wild-type	wild-type	impaired	wild-type	impaired	impaired

1013

1014

1015

1016

1017

1018

1019

1020

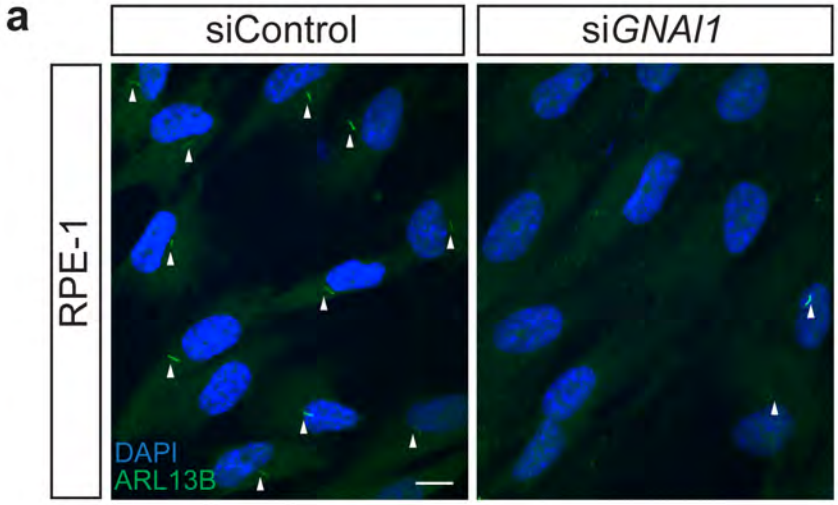
a
siControl
siGNAI1
RPE-1
DAPI
ARL13B

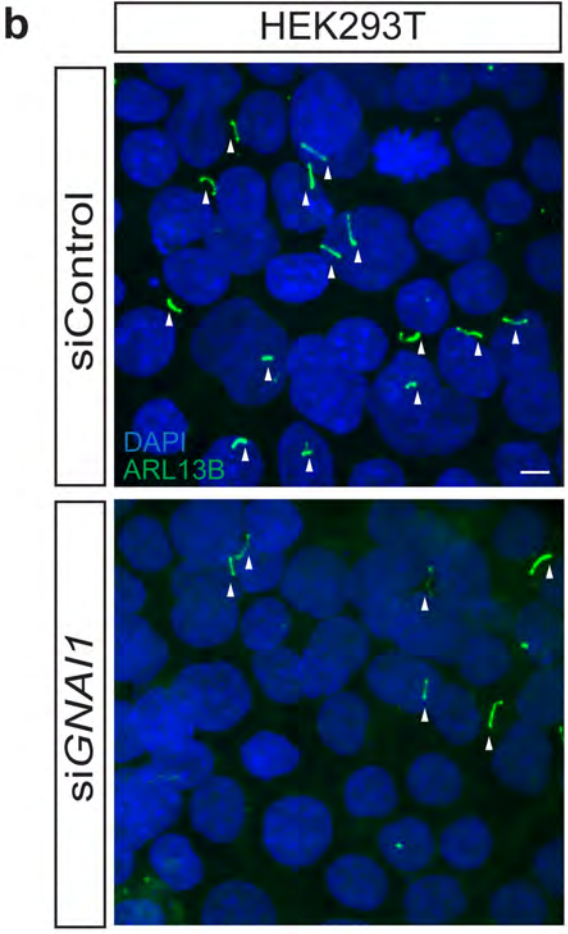
b
HEK293T
siControl
siGNAI1
DAPI
ARL13B

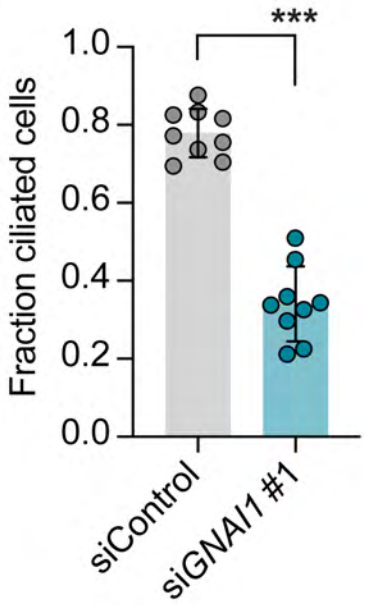
c
***
Fraction ciliated cells
1.0
0.8
0.6
0.4
0.2
0.0
siControl
siGNAI1 #1

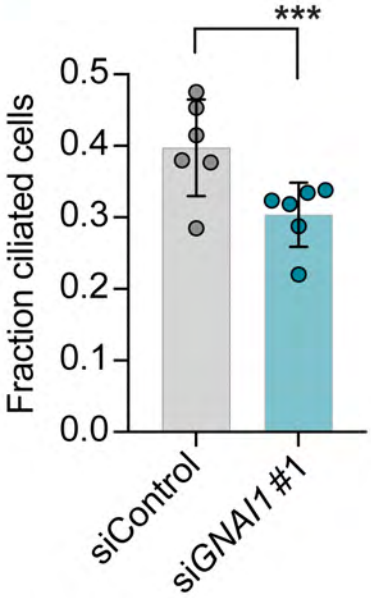
d
***
Fraction ciliated cells
0.5
0.4
0.3
0.2
0.1
0.0
siControl
siGNAI1 #1

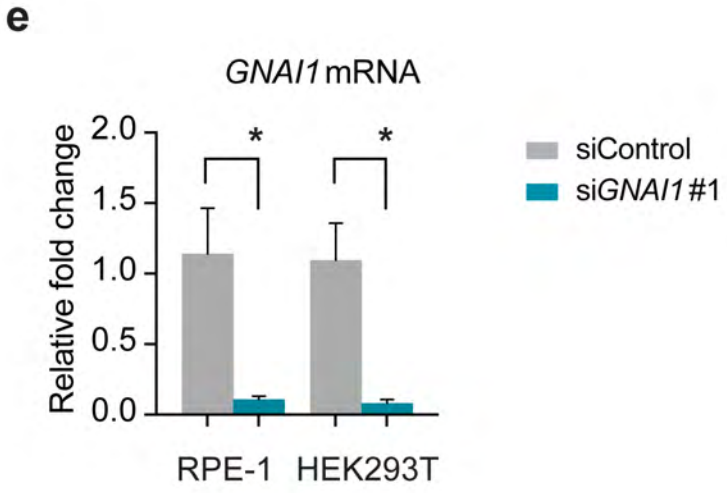
e
GNAI1 mRNA
Relative fold change
2.0
1.5
1.0
0.5
0.0
*
*
RPE-1
HEK293T
siControl
siGNAI1 #1

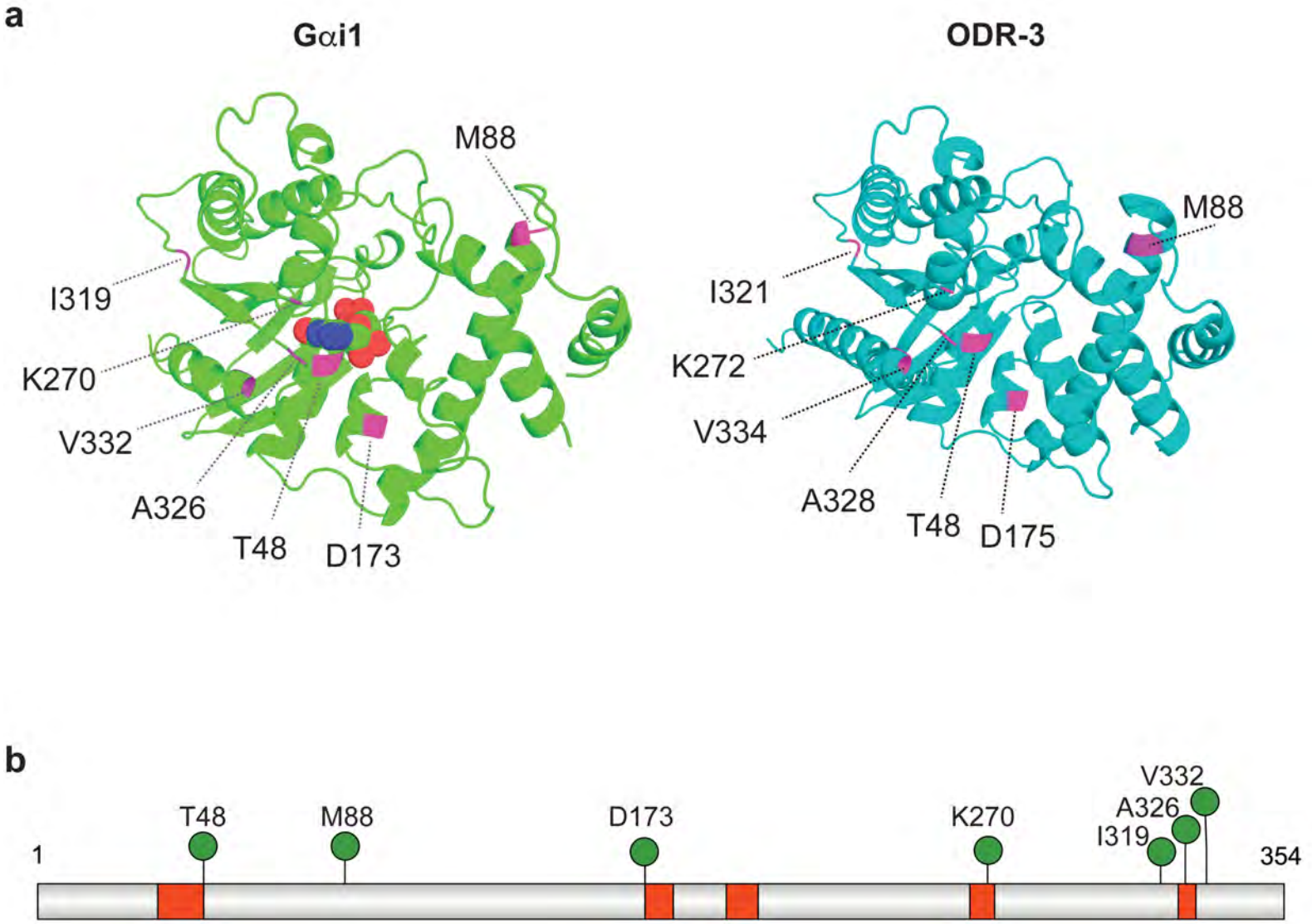
a
Gαi1
ODR-3
M88
I319
K270
V332
A326
T48
D173
M88
I321
K272
V334
A328
T48
D175
b
T48
M88
D173
K270
V332
A326
I319
1
354

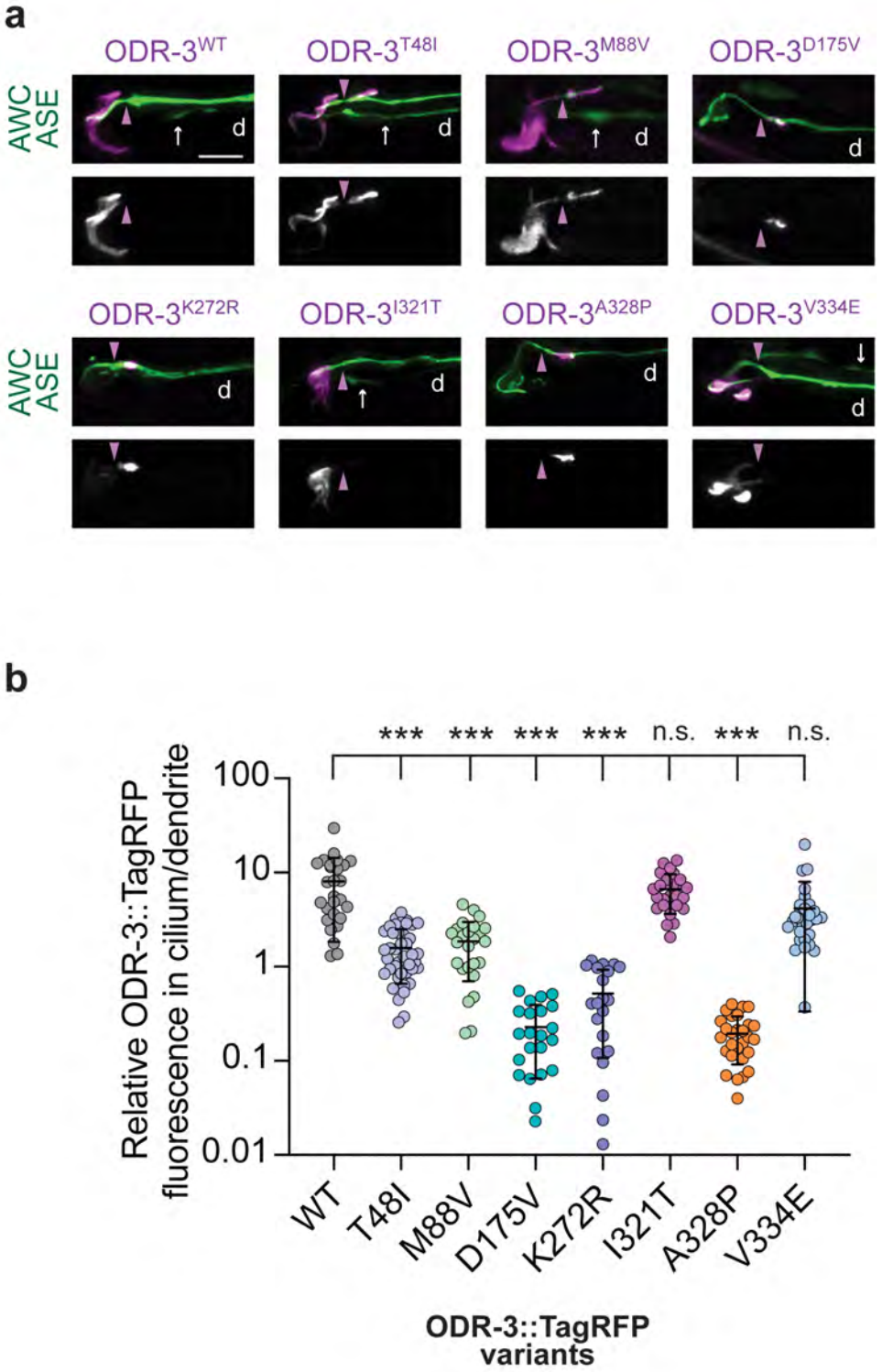
a
ODR-3WT
ODR-3T48I
ODR-3M88V
ODR-3D175V
AWC
ASE
d
ODR-3K272R
ODR-3I321T
ODR-3A328P
ODR-3V334E
b
*** *** *** *** n.s. *** n.s.
Relative ODR-3::TagRFP fluorescence in cilium/dendrite
100
10
1
0.1
0.01
WT
T48I
M88V
D175V
K272R
I321T
A328P
V334E
ODR-3::TagRFP variants

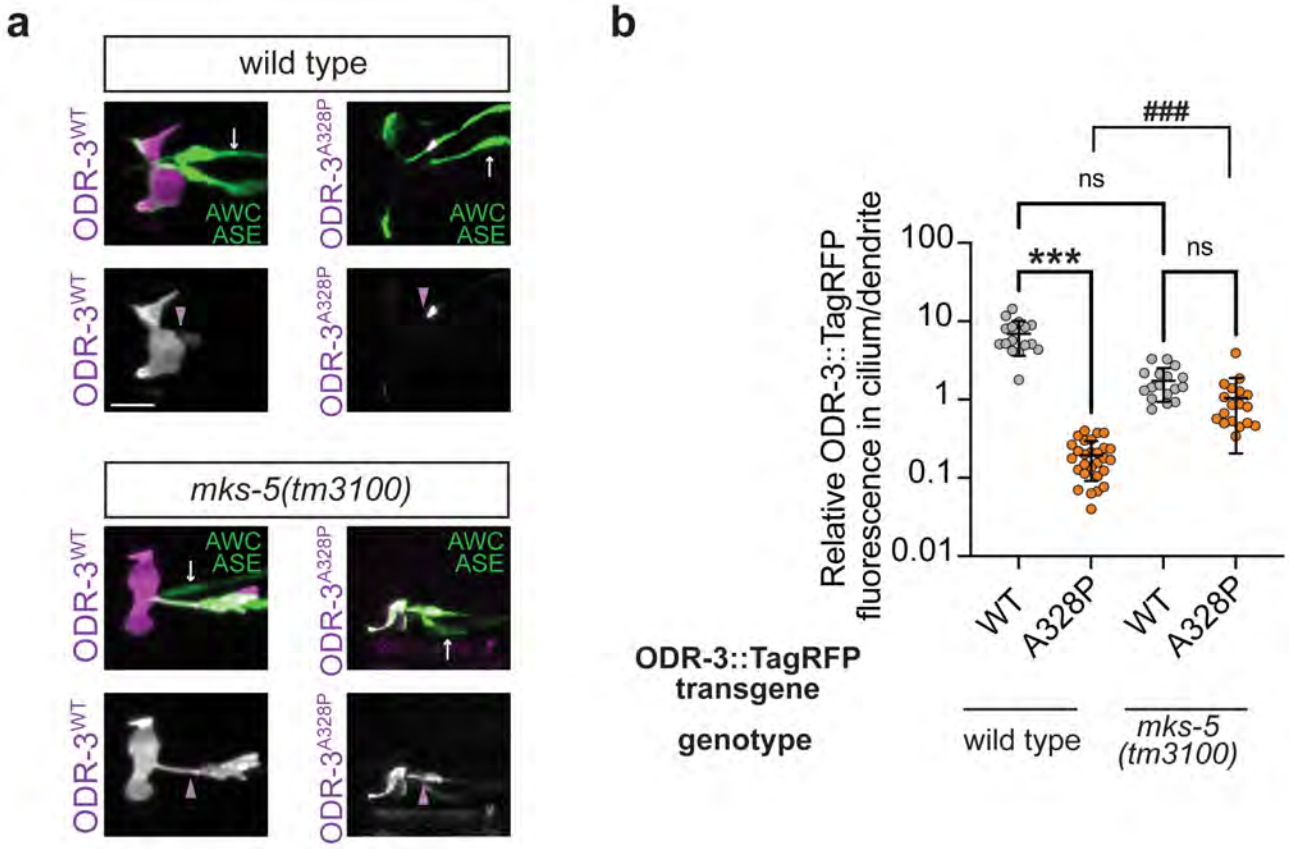
a
wild type
ODR-3WT
ODR-3A328P
AWC
ASE
mks-5(tm3100)
b
Relative ODR-3::TagRFP fluorescence in cilium/dendrite
100
10
1
0.1
0.01
***
ns
ns
###
WT
A328P
WT
A328P
ODR-3::TagRFP transgene
genotype
wild type
mks-5 (tm3100)

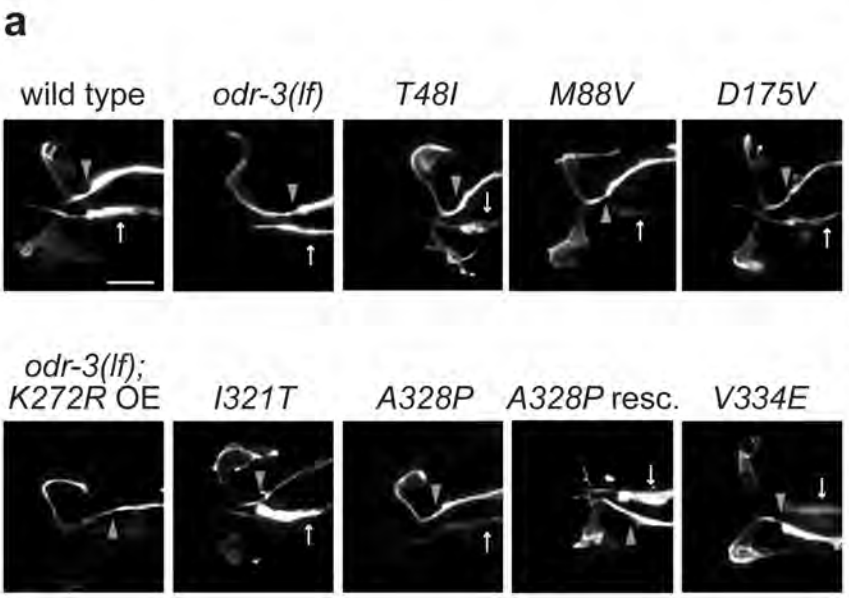
a
wild type
odr-3(lf)
T48I
M88V
D175V
odr-3(lf); K272R OE
I321T
A328P
A328P resc.
V334E

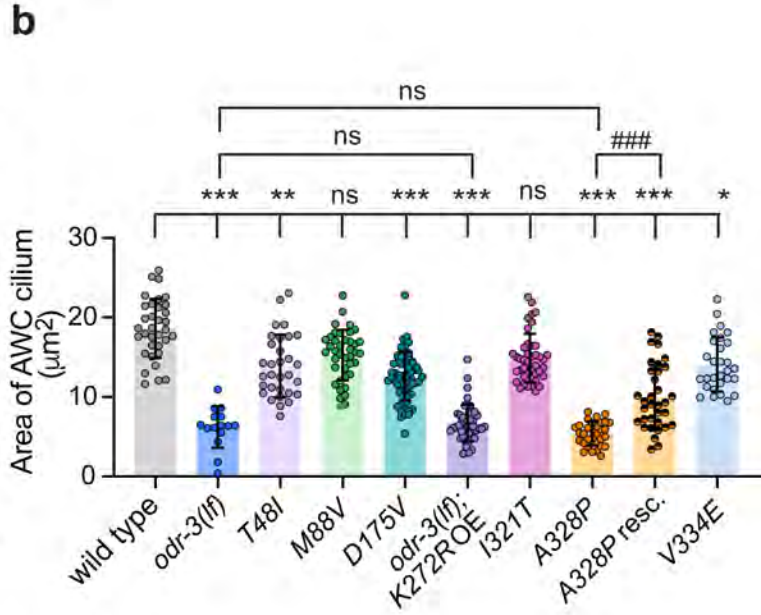
b
Area of AWC cilium (μm²)
30
20
10
0
ns
ns
###
*** ** ns *** *** ns *** *** *
wild type
odr-3(lf)
T48I
M88V
D175V
odr-3(lf); K272R OE
I321T
A328P
A328P resc.
V334E

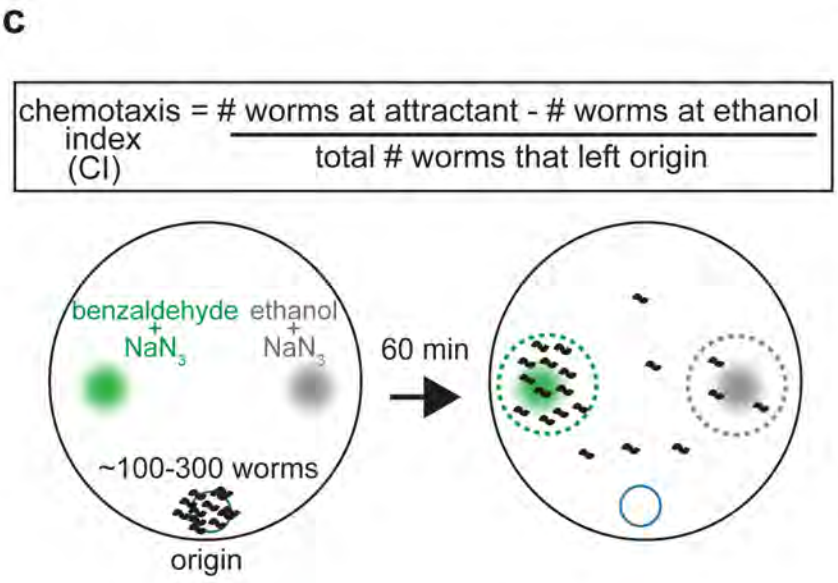
c
chemotaxis index (CI) = # worms at attractant - # worms at ethanol / total # worms that left origin
benzaldehyde + NaN3
ethanol + NaN3
~100-300 worms
origin
60 min

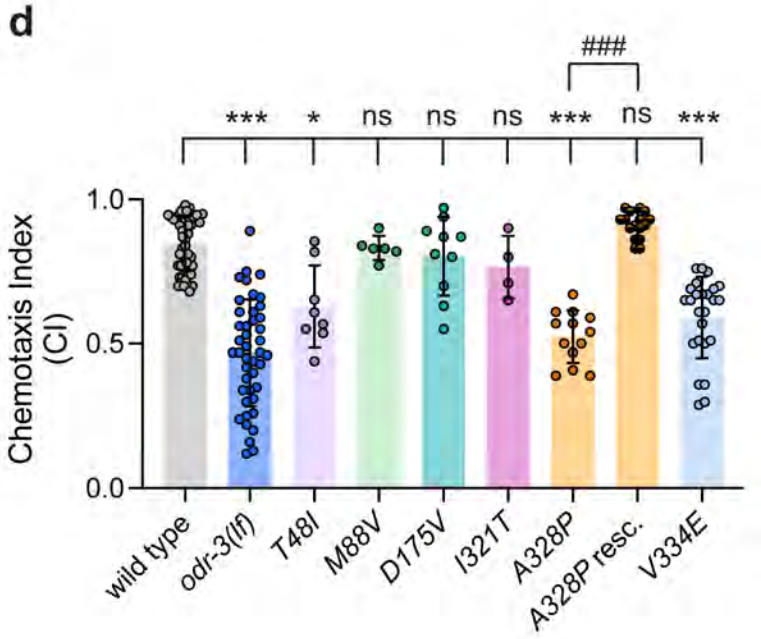
d
Chemotaxis Index (CI)
1.0
0.5
0.0
###
*** * ns ns ns *** ns ***
wild type
odr-3(lf)
T48I
M88V
D175V
I321T
A328P
A328P resc.
V334E

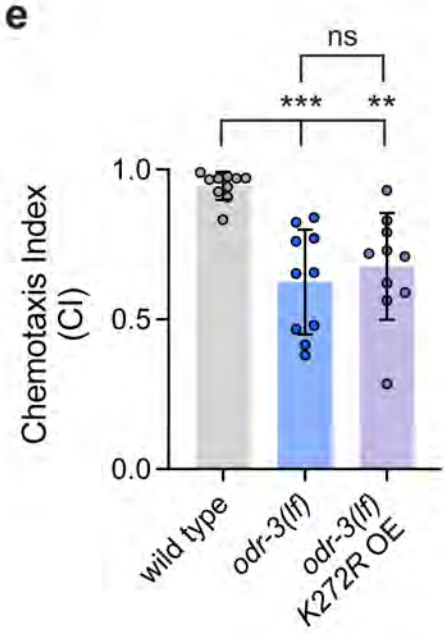
e
Chemotaxis Index (CI)
1.0
0.5
0.0
ns
*** **
wild type
odr-3(lf)
odr-3(lf) K272R OE

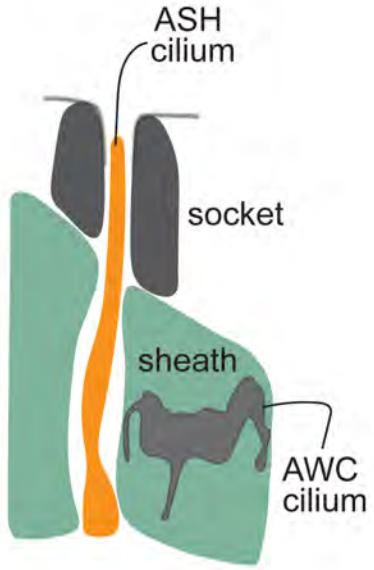
a
ASH
cilium
socket
sheath
AWC
cilium

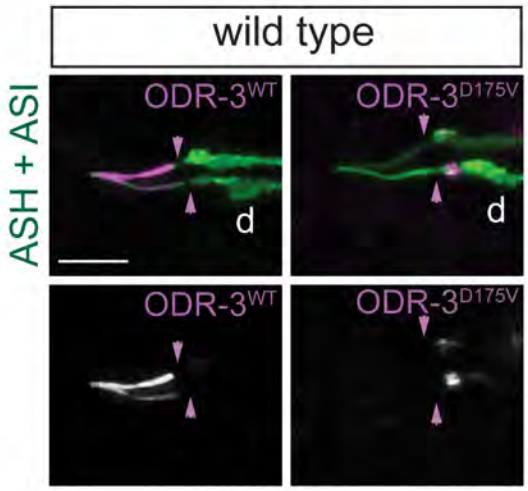
b
wild type
ASH + ASI
ODR-3WT
ODR-3D175V
d
d
ODR-3WT
ODR-3D175V

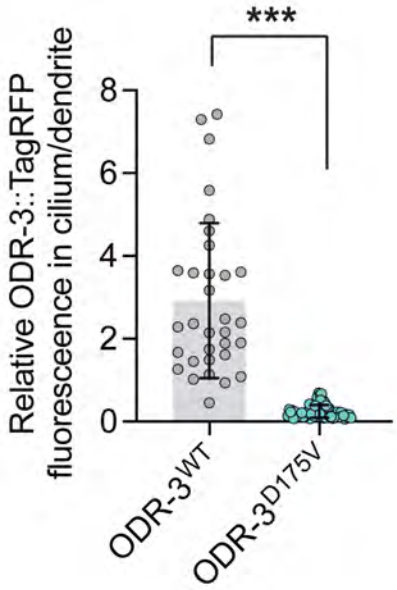
c
***
Relative ODR-3::TagRFP
fluorescence in cilium/dendrite
8
6
4
2
0
ODR-3WT
ODR-3D175V

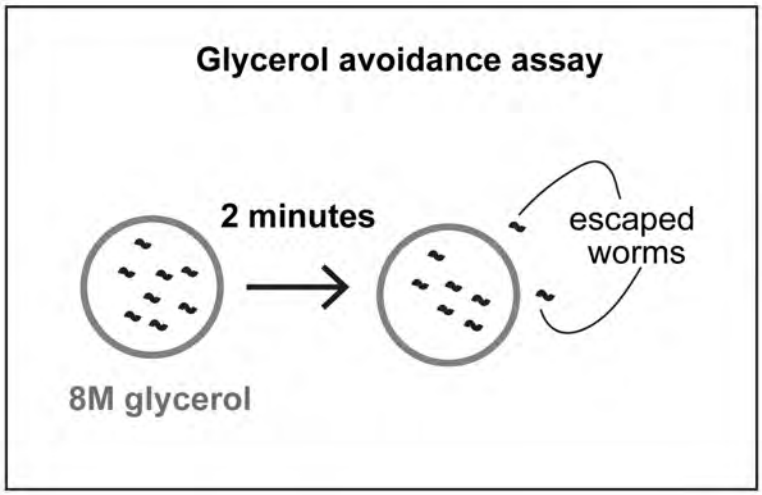
d
Glycerol avoidance assay
2 minutes
escaped
worms
8M glycerol

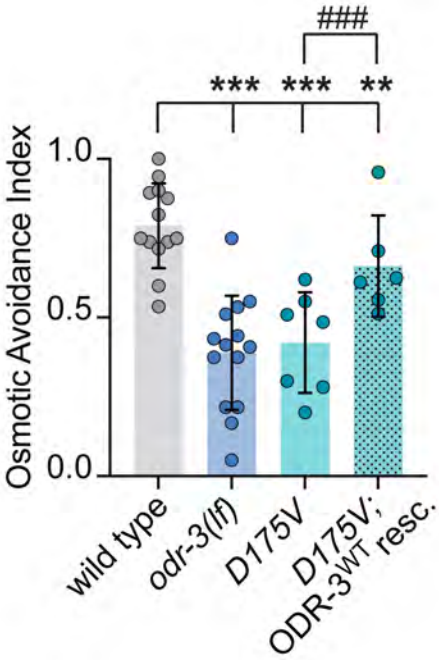
e
###
***
***
**
Osmotic Avoidance Index
1.0
0.5
0.0
wild type
odr-3(lf)
D175V
D175V;
ODR-3WT resc.

a

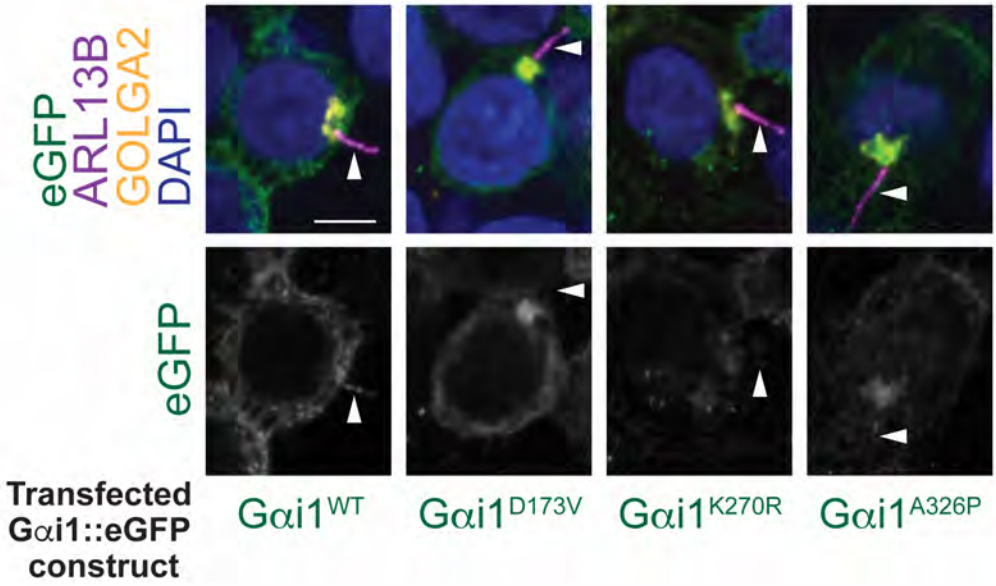
eGFP
ARL13B
GOLGA2
DAPI
eGFP
Transfected Gαi1::eGFP construct
Gαi1WT
Gαi1D173V
Gαi1K270R
Gαi1A326P

b

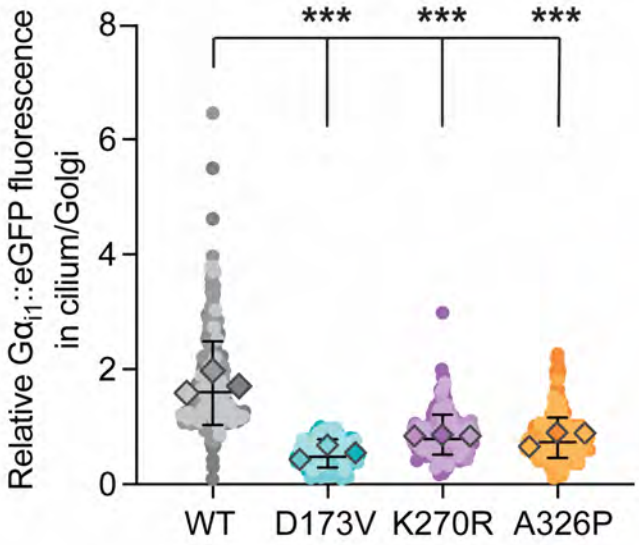
Relative Gαi1::eGFP fluorescence in cilium/Golgi
8
6
4
2
0
***
***
***
WT
D173V
K270R
A326P